Dissertationes Forestales 368

Critical aspects in trafficability of forest terrain and gravel roads

Ville Karjalainen
School of Forest Sciences
Faculty of Science, Forestry and Technology
University of Eastern Finland

Academic dissertation

To be presented, with the permission of the Faculty of Science, Forestry and Technology of the University of Eastern Finland, for public criticism in the auditorium Natura 100 of the University of Eastern Finland, Yliopistokatu 7, Joensuu, on the 30th of May 2025, at 12 o' clock noon.

Title of dissertation: Critical aspects in trafficability of forest terrain and gravel roads
Author: Ville Karjalainen

Dissertationes Forestales 368
https://doi.org/10.14214/df.368

Thesis supervisors:
Professor Timo Tokola
School of Forest Sciences, University of Eastern Finland, Finland

Research Director Jukka Malinen
Metsäteho Oy, Vantaa, Finland

Pre-examiners:
Professor Jori Uusitalo
University of Helsinki, Faculty of Agriculture and Forestry, Department of Forest Sciences, Helsinki Finalnd

Research Director Hannu Hyyppä
Research Institute of Measuring and Modelling for the Built Environment, Aalto University, Espoo, Finland

Opponent:
Docent Tuomo Kauranne, D.Sc. (For.)
Arbonaut Oy, Joensuu, Finland

ISSN 1795-7389 (online)
ISBN 978-951-651-826-1 (pdf)

Publishers:
Finnish Society of Forest Science
Faculty of Agriculture and Forestry of the University of Helsinki
School of Forest Sciences of the University of Eastern Finland

Editorial Office:
Finnish Society of Forest Science
Viikinkaari 6, FI-00790 Helsinki, Finland
http://www.dissertationesforestales.fi

Karjalainen, V. (2025) Critical aspects in trafficability of forest terrain and gravel roads. Dissertationes Forestales 368. 68 p. https://doi.org/10.14214/df.368

ABSTRACT

The forest industry in Finland faces challenges in maintaining a year-round supply of fresh roundwood due to low bearing capacity in forest terrain and roads during certain seasons. The accessibility of forest terrain depends on the physical properties of the soil, which in turn impacts the cost-effectiveness and quality of mechanized forest operations. However, the resolution of currently available trafficability data is insufficient for accurate stand-specific operational planning. Similarly, only a limited number of forest roads can support heavy-duty vehicles year-round, and manual assessments of road conditions are time-consuming. Thus, improved methods utilizing readily available data for route planning and targeted road maintenance are required. The objective of this thesis is to explore methodologies for predicting terrain mobility and forest road bearing capacity, particularly using gamma-ray spectrometry.

The thesis comprises three sub-studies using soil and forest road data alongside gamma-ray datasets from Eastern Finland. The first and third studies focus on predicting small-scale soil property changes (stoniness, soil depth, peat depth) using airborne and ground-based gamma-ray measurements. The third study also examined the correlation between airborne and ground-based gamma-ray datasets. Ordinal regression and linear discriminant analysis were employed as analytical methods in these studies. The second study focuses on predicting forest road bearing capacity using easily measurable road and terrain properties, applying linear mixed-effects models.

The third study revealed a weak correlation between airborne and ground-based gamma-ray datasets. The first and third studies showed promising results in predicting soil properties using gamma-ray datasets, with up to 70% accuracy in stoniness and soil depth predictions. The second study showed moderate success in predicting forest road bearing capacity using easily measurable field data, achieving accuracy of 34% and RMSE% of 36%. Overall, the findings highlight the potential of gamma-ray spectrometry in enhancing the prediction of soil properties and forest road bearing capacity.

Keywords: Trafficability, bearing capacity, forest terrain, forest roads, gamma-ray spectrometry, falling-weight deflectometer

ACKNOWLEDGEMENTS

I would like to express my sincere gratitude to my supervisors, Professor Timo Tokola and D.Sc. Jukka Malinen, for their invaluable guidance and support throughout this journey. Special thanks to Professor Tokola for providing me with the opportunity to work on this topic across several projects during my doctoral studies. I am also grateful to my pre-examiners and to my dear colleagues at the University of Eastern Finland for their encouragement and insights. I would like to thank Professor Heli Peltola and the UNITE project for funding my research during my time at the university. My appreciation extends to the Doctoral School of the University of Eastern Finland for their financial support in 2020–2021, and to the Finnish Cultural Foundation for their funding in 2020 and 2023. Lastly, I am deeply thankful to my family and friends for their unwavering support and encouragement throughout this long and rewarding process.

Kuopio, 14th of April 2025

Ville Karjalainen

LIST OF ORIGINAL ARTICLES

This thesis is based on data presented in the following articles, referred to by Roman Numerals I-III.

I Karjalainen V., Tokola T., Malinen J. 2022. Prediction of topsoil stoniness using soil type information and airborne gamma-ray data. Canadian Journal of Forest Research. 52(1): 27-37. https://doi.org/10.1139/cjfr-2021-0001

II Karjalainen, V., Malinen, J., Tokola, T. 2024. Predicting bearing capacity and trafficability classes of forest roads using road properties and surrounding terrain information. *Road Materials and Pavement Design*, 1–18. https://doi.org/10.1080/14680629.2024.2434945

III Karjalainen, V., Malinen, J., Tokola, T. 2024. Comparison of two gamma-ray datasets measured with different methods and assessment of their performance to predict soil properties. *International Journal of Forest Engineering*, *36*(1), 29–42. https://doi.org/10.1080/14942119.2024.2398947

Ville Karjalainen was responsible for collecting the field data, as well as performing all calculations and analyses in all three papers. He also served as the corresponding author for each of the papers. Timo Tokola and Jukka Malinen provided supervision and guidance throughout the writing process and commented on the manuscripts prior to submission for review.

TABLE OF CONTENT

ABBREVIATIONS

Air gamma	Airborne based gamma spectrometry measurement
ALS	Airborne laser scanning
ANOVA	Analysis of variance
CRP	Close-Range Photogrammetry
DEM	Digital Elevation Model
DCP	Dynamic cone penetrometer
DI	Ditch index
DTM	Digital terrain model
DTW	Depth-to-water index
FT	Fine-till
FWD	Falling weight deflectometer
GPS	Global Positioning System
Ground gamma	Ground based gamma spectrometry measurement
GSF	Geological survey of Finland
K	Potassium
LDA	Linear discriminant analysis
LFWD	Light falling weight deflectometer
LiDAR	Light detection and ranging
LME	Linear mixed effects
LOOCV	Leave-one-out cross-validation
MD%	Mean difference (relative)
MLS	Mobile laser scanning
MN/m^2	Meganewton per square meter
RMSE%	Root mean squared error (relative)
RW	Roadway width
SI	Stoniness index
SIC	Stoniness index class
ST	Sandy-till
Th	Thorium
TLS	Terrain laser scanning
U	Uranium
UAV	Unmanned aerial vehicle
URW	Useable road width
VIF	Variance inflation factor

1 INTRODUCTION

1.1 Background

According to the Natural Resources Institute of Finland (2024), approximately 61.0 Mm^3 (million cubic meters) of wood with the dimensions of saw logs or pulpwood and 4.9 Mm^3 of energy wood were harvested in Finland in 2023 for use by the forest industry. In our constantly changing climate, winter harvesting conditions can vary greatly from year to year, making it difficult to plan harvesting operations in advance. The mills aim to maintain a year-round continuous flow of fresh roundwood, which is a major challenge during low bearing capacity seasons in Finland. During the early and late winter months, the soil is only partially frozen, and the terrain and forest roads are particularly sensitive to heavy-duty vehicle traffic. Conducting detailed on-site inspections is costly, and weather conditions are subject to rapid and frequent change during these seasons.

Mechanized wood harvesting requires adequate trafficability conditions for forest tractors and operations are avoided during periods of high soil failure risk. Consequently, harvesting is often postponed to the winter season, when soil is typically frozen (Pohjankukka et al. 2016). Moreover, within the existing forest network there is a limited number of roads that are suitable for year-round use by heavy-duty vehicles. Venäläinen et al. (2018) estimated that the seasonal variation in timber procurement causes costs amounting to approximately 70M € every year largely on account of frost heave and other bearing capacity constraints, restrictions on the accessibility of stands and demand fluctuations at the mills. The costs caused by challenging trafficability conditions could be reduced by obtaining additional information on soil and road conditions, especially their bearing capacity (Pohjankukka et al. 2016).

1.2 Trafficability of forest terrain

Interest in small-scale variations in soil characteristics and terrain topography has increased in recent times due to the challenges posed by varying weather conditions during rainy spring and autumn periods and the unfrozen state of the soil in some places during the winter. A major challenge for Nordic forestry is to maintain constant but high-quality harvesting with capital-intensive harvesting machinery and still finish the operations with acceptable negative impacts on the soil and without any unexpected difficulties (Sirén et al. 2019). The number of seasonal factors involved in harvesting operations reflects concerns about soil erosion, rutting, and compaction as well as the prevention of tree diseases and various forms of damage from heavy vehicles (Geisler et al. 2016). Forest certification standards guide loggers towards keeping damage to a minimum. In addition to the climatic factors, rut formation is affected by the bearing capacity of the soil, the characteristics of the machinery used in harvesting and hauling, and the experience of the operator (Suvinen et al. 2009).

Both trafficability and rut formation depend on the ability of the soil to resist the force exerted on it by a rotating tyre or roller (Saarilahti, 2002). Nordic research has examined the factors influencing rut formation, with several studies highlighting the significance of soil properties, the mass or wheel load of the tractor, and the characteristics of the wheels, chains, and tracks (Saarilahti and Anttila, 1999; Bygdén et al. 2003; Eliasson L, 2005; Uusitalo et al. 2015; Palander and Kärhä, 2016; Mattila and Tokola, 2018; Sirén et al. 2019; Ala-Ilomäki et

al. 2020; Uusitalo et al. 2020). The utilization of heavy machinery in forest harvesting operations has been demonstrated to result in soil compaction, thereby reducing soil porosity, water infiltration rates, and nutrient availability. Vehicle loads that exceed the soil's strength have been shown to not only cause soil damage but also damage to trees, predominantly to their roots, and occasionally to the stem, due to the increase of uncontrolled movement of the forwarder (Pohjankukka et al. 2016). The progressive effect of machine passes can differ significantly according to the physical properties and depth of the soil and depends strongly on the soil texture (Cambi et al. 2015).

GIS-based modelling has been offered as a means to predict terrain mobility conditions in support of the planning of forest operations (Suvinen, 2006; Suvinen et al. 2009). To avoid soil damage, operators require precise information regarding soil and site conditions. The ability to reliably identify individual soil and terrain properties (e.g., stoniness, as well as soil and peat layer thickness) would significantly assist in the estimation of terrain trafficability and help to further develop the existing terrain trafficability maps (Metsäkeskus, 2023; Finnish Meteorological Institute, 2023). By observing the geomorphological properties of the soil, such as wetness, soil type, and stoniness, at a small-scale level, one could plan routes for heavy harvesting machinery to pass through areas where these soil properties are optimal in terms of high bearing capacity. In general, the bearing capacity decreases as the grain-size of the soil becomes finer and the number of boulders and stones diminishes. However, stoniness may also reduce machine mobility.

Optimizing trafficability in forest terrain is dependent upon effective operation planning and high-resolution terrain modelling. Site-specific planning and operational practices, such as the selection of appropriate harvesting methods, routes, and equipment, can minimize environmental impact and reduce soil compaction. High-resolution terrain mapping and modeling techniques, including LiDAR, aerial imagery, and gamma-ray spectrometry, can provide detailed information about terrain characteristics, such as slope, elevation, surface roughness, and soil wetness. This information can be used to identify areas with favorable trafficability conditions and plan harvesting operations accordingly. In addition, the design of harvesting machinery, such as tracks instead of wheels, articulated frames, and low-pressure tires, can improve traction and maneuverability and reduce rut formation in challenging terrain conditions.

Predicting trafficability in forest terrain poses several challenges, primarily due to the complex and dynamic nature of natural environments. Variability in terrain conditions, such as soil moisture, vegetation growth, and seasonal changes, can significantly affect trafficability and make predictions less reliable. Factors such as vehicle type, load weight, operator skill, and mission objectives can influence the perceived difficulty of traversing forest terrain and may not always be captured accurately by predictive models. To ensure the efficacy of trafficability prediction, human decision-making processes, including route planning and risk assessment, must be considered alongside terrain characteristics. Several methods are employed to predict the trafficability of forest terrain, ranging from empirical models to remote sensing techniques. Empirical models often utilize terrain attributes such as slope, soil type, vegetation density, and surface roughness to estimate trafficability. These models may be based on field measurements, historical data, or expert knowledge.

1.3 Stoniness of forest soil and effect on forest operations

The stoniness of Finnish forest soil exerts profound ecological impacts, influencing soil structure, nutrient cycling, and habitat diversity. Stones embedded within the soil affect soil porosity, water infiltration rates, and drainage patterns, which, in turn, influence plant growth and ecosystem productivity. The stoniness of Finnish forest soil poses both challenges and opportunities for forest management practices. Soil preparation, reforestation, and road construction can be hindered by stony soils, leading to increased costs and operational challenges. However, the stoniness of forest soil also presents opportunities for route planning of logging machinery in low bearing capacity areas reducing rut formation but on the contrary, it may increase soil compaction.

The incidence of stones and boulders is an important forest soil property, affecting the hydrology of a site, the soil temperature, the amount of available nutrients, and hence the potential for timber production (Viro, 1947; Ashby et al. 1984; Eriksson and Holmgren, 1996). The stoniness of the topsoil also has a major impact on several forest operations, such as harvesting, forwarding and soil preparation.

The basic precondition for reforestation is well-planned and executed soil preparation, so that, when successful, the effects will be reflected in the forest yield over the entire rotation period (Immonen et al. 2000). In the context of forest regeneration, the most relevant measure is the stoniness of the soil at depths of 20–30 centimeters (Melander et al. 2019). The stone content of the topsoil is particularly important when planning forest regeneration, since it can often render soil preparation challenging and detract from the overall quality of the work. A high stone content can cause difficulties for both soil preparation and planting, and in some areas proper soil preparation may become impossible or be only partially successful (Saarinen, 2006; Luoranen et al. 2007; Rantala et al. 2010; Lideskog et al. 2014; Saksa et al. 2018; Melander et al. 2019).

The choice of soil preparation method depends on the thickness of the soil layer, the soil type, the stoniness of the soil, the current conditions of the forest site, and the tree species being planted (Luoranen et al. 2007; Löf et al. 2012; Äijälä et al. 2014). The main soil preparation methods, including harrowing (disc trenching), patch scarification and mounding (Löf et al. 2012), all involve tilling the forest soil in some manner, but at different depths and in different patterns. Mounding is an example of a forest regeneration process that would benefit from knowing the prevailing stoniness of the target site, at least when the continuous mounding method is considered (Rantala et al. 2010; Saksa et al. 2018).

In Finland, most forest soils are tills of various types, and stoniness is one of their peculiarities. It has been reported that the volume of coarse fragments in forest soils, i.e. their stoniness (Viro, 1947), is substantial, e.g. averaging 42.3% by volume in Finland (depths of 0 – 30 cm) (Viro, 1958) and 49.5% in Sweden (depths of 0 – 40 cm) (Eriksson and Holmgren, 1996), whereas many rut formation and trafficability studies conducted elsewhere focus on homogeneous, deep soils such as peatlands and very few of them focus on predicting the key soil characteristics that determine its bearing capacity.

However, topsoil stoniness data are not available in any existing map database, and traditional measurements of soil stoniness have always required laborious soil penetration methods.

1.4 Finnish forest road network

Finland has one of the densest forest road networks in Europe, with approximately 160,000 km of forest roads (6–16.5 m/ha, Uotila and Viitala, 2000), built to serve the transportation needs of the forest industry, the silvicultural management of forests, and others such as recreational users and rescue services. The Finnish forest road network was mainly constructed between 1960 and 1990, and the planned structural life of the roads was 20–30 years. As a result, the majority of these roads are now reaching the end of their life cycle (Kaakkurivaara and Uusitalo, 2011). Moreover, the requirements for forest roads have changed significantly since the time they were originally constructed, largely due to the increased weight of timber trucks. In 1960, the maximum weight capacity for timber trucks was 30 tons; however, the current weight limit is 76 tons. Timber trucks are the most common method of transporting timber because they offer flexible, low-cost transportation to constantly changing locations. In 2014, Malinen et al. estimated that approximately 40 Mm^3 of timber is transported to mills by trucks each year, with nearly all logistics chains beginning from low-volume road networks. That amount has increased since then. A well-functioning network of forest roads is therefore needed to ensure a reliable flow of fresh roundwood to the mills.

Forest roads are often constructed from materials available at the site, with some materials transported from elsewhere. The structure of forest roads is generally divided into two major parts: subgrade and pavement. The subgrade consists of materials available on site, such as soil obtained during ditch excavation, and forms the underlying structural layer of the road. The pavement is constructed on top of the subgrade and typically includes three sub-layers: the surface layer, the base course layer, and the sub-base layer. The sub-base layer, usually composed of coarse material such as gravel, separates the upper pavement layers from the subgrade and helps prevent the capillary rise of water. The base course layer typically consists of crushed rock, while the surface layer is made of either crushed rock or finer gravel.

The majority of old forest roads were built without properly constructed structural layers (i.e., sub-base and base course layers) to prevent capillary moisture. Consequently, these roads often have low bearing capacity during thaw seasons. Many such roads negatively affect the functionality and efficiency of the transportation network and are in need of renovation (Kaakkurivaara and Uusitalo, 2011). In areas where the ground is frozen for part of the year, the surface stiffness of a forest road is significantly reduced during thaw periods, resulting in lower bearing capacity and an increased risk of structural damage if subjected to heavy traffic (Huvstig, 2012; Kaakkurivaara et al. 2015; Saarenketo and Aho, 2005). This issue is currently addressed by restricting heavy traffic on such roads. The number of road sections with bearing capacity restrictions varies yearly, peaking during the spring thaw, typically from April to June (Saarenketo and Aho, 2005; Vuorimies et al. 2015). Due to reduced bearing capacity and fewer trafficable roads, the average distance from accessible roadside timber stores to the mills may increase, as timber must be transported from beyond the normal procurement areas of mills. However, with relatively small improvement investments, the quality of these roads could be enhanced to withstand timber transportation even during thaw periods.

Still, it is not economically sensible to renovate all such roads. The scale of renovations must be considered based on the weight of the trucks used, the intensity of road use, and the season during which the road is used (Kaakkurivaara et al. 2016; Korpilahti, 2008). According to Viitala et al. (2004), the profitability of a renovation investment depends on the volume and timing of fellings in the area served by the road. It is important to note that a

forest road is only as good as its weakest point in terms of trafficability—i.e., one weak segment with low bearing capacity can prevent the use of the entire road. By identifying and targeting these weak points for renovation, road quality could be improved with relatively small investments (Viitala et al. 2004; Korpilahti, 2008; Kaakkurivaara and Korpunen, 2017).

It is anticipated that climate change will significantly affect the bearing capacity and trafficability of forest roads, with differing impacts across Finland's regions. The occurrence of winter storms, strong winds, and increased precipitation is likely to disrupt transportation, increase the risk of structural damage, and shorten road lifespans—posing challenges for road maintenance (Malinen et al. 2014; Saarelainen and Makkonen, 2007). In Southern Finland, temperatures will rarely remain below 0°C for extended periods, preventing roads from freezing properly and decreasing the number of days with sufficient bearing capacity for winter transportation. Additionally, high moisture content will continually affect the surface and structure of forest roads, further reducing bearing capacity. Conversely, in Central and Northern Finland, increased snowfall is expected to cause difficulties in winter maintenance (Malinen et al. 2014; Vuorimies et al. 2019). On the other hand, Saarelainen and Makkonen (2007) note that climate change may also have positive effects on timber transportation, as milder winters could reduce frost depths in forest roads, thereby shortening the length of the spring thaw. According to Sterner et al. (2023), the two most significant challenges are the fluctuating weather conditions and the decreased accessibility of forest roads, which have a considerable impact on wood supply and increase the work intensity required for transportation.

1.5 Road inventories and assessment of quality

Trafficability and bearing capacity are two important factors that depict the quality of forest roads. Bearing capacity describes the stiffness of a forest road, and it is often used when assessing the usability of forest roads. The bearing capacity of forest roads describes the ability to withstand traffic without causing rutting or damage to the road structure. Information regarding a road's bearing capacity can be utilized to assess whether the road requires repairs or if it possesses the structural integrity to withstand traffic during thaw periods (trafficability). While bearing capacity and trafficability are closely related, they should not be confused. Trafficability refers to the period during which a road can support typical transport volumes—especially by heavy timber trucks—without significant rutting or deformation. Trafficability can be estimated from bearing capacity and elasticity measurements, but it is a distinct concept focused on seasonal usability. The trafficability of forest roads is typically classified according to seasons when the road can withstand the passage of timber trucks weighing 75 tons. The most commonly utilized classifications are: **All-year** category roads are trafficable throughout the year, even during periods of spring thaw and autumn, when precipitation levels are high. **Summer** category roads are trafficable in summer and winter, and partially manage to maintain their bearing capacity to avoid significant rutting even during the autumn, However, these roads are unable to withstand traffic during spring thaw. **Dry Summer** category roads are trafficable in winters and in exceptionally dry summers with prolonged heat waves and little precipitation. **Winter** category roads are trafficable only when the road structure is frozen to a sufficient depth.

The most widely used method of measuring the bearing capacity of forest roads is through the use of a falling weight deflectometer (FWD) or a light falling weight deflectometer (LFWD). These devices have been shown to effectively replicate the wheel load of a truck,

making them useful tools for assessing the load-bearing capabilities of a road surface (George 2003; Kaakkurivaara et al. 2015). The FWD and LFWD are frequently used on paved low-volume roads and on forest roads in Finland (Saarenketo and Aho 2005). Another widely used tool is the dynamic cone penetrometer (DCP), which measures soil strength based on penetration resistance. It uses a cone tip that is driven into the ground, and results can be correlated with factors such as soil moisture and density (Kaakkurivaara et al., 2015). Numerous studies support the use of DCP in evaluating forest roads (Dai and Kremer, 2005; Embacher, 2006; Mohammadi et al., 2008; Siekmeier et al., 2009). There is also a strong correlation between DCP and FWD results (George & Uddin, 2000; George, 2003). However, while these measurements provide high-quality data on road surface bearing capacity (MN/m^2) and trafficability, they are not feasible for widespread, large-scale applications. It would be beneficial to identify variables that could be used to provide information on road quality and trafficability without FWD measurements.

The overall trafficability of a forest road is affected by several characteristics which are often assessed along with surrounding terrain properties when reviewing the road's condition. The bearing capacity will remain good if the road structures are dry and rain or meltwater is prevented from accumulating on the surface or in the ditches close to the road frame. The most significant factors affecting the moisture of the road surface are curbs, shoulders, and potholes. Insufficient slope on the road surface can lead to rutting and the formation of pits, curbs, and banks from loose road material deposited beside the roadway. When these properties are met, water will flow freely into the roadside ditches and the road surface will remain dry, thereby reducing the risk of impaired surface bearing capacity. The surface layer of the road must be composed of a suitable material, most often crushed gravel or crushed rock, to ensure adequate stiffness and bearing capacity. Waga et al. (2015) found that wear and smoothness had the most effect on the overall quality of a road surface in terms of trafficability. The determination of surface quality is a particularly challenging yet crucial aspect in road evaluation. Roadside ditches play an important part in directing water away from the vicinity of the road structure and into the main drainage ditches. For effective drainage, the ditches must be sufficiently deep and unobstructed (i.e., free of trees and stones). The depth of the ditches will usually correlate with the type of soil surrounding the road. For instance, the presence of fine-grained soils and peat necessitates the construction of deeper ditches, whereas coarse soil types permit shallower ditches (see Waga et al. 2020). The ability to direct water away from the road surface and frame is a crucial aspect of the maintenance of forest roads, as effective drainage can markedly reduce thawing problems (Korpilahti, 2008).

Forest road inventories are mainly carried out through field assessments using existing guidelines. While certain parameters can be objectively measured, others require subjective evaluation, thereby allowing the exercise of individual discretion. The subjective evaluation process demands a high degree of expertise to ensure accuracy and can introduce a risk of autocorrelation when assessing multiple subjective characteristics within the same road. Forest road inventories require an assessment of numerous characteristics which is both laborious and time-consuming when conducted on a large scale through fieldwork. Conducting these road quality assessments, especially on private roads, is critical for infrastructure management. The limited publicly available information regarding these roads complicates the planning of timber transportation, thereby underscoring the necessity for such assessments. As previously mentioned, the execution of these quality assessments requires a significant degree of technical expertise to collect reliable information. This, in turn, impedes the possibility of conducting a large-scale data collecting carried out by

individual road owners. It is therefore essential to develop faster methods of identification by employing data that is readily available or easily accessible. The utilization of readily available open data and remote sensing, such as airborne laser scanning (ALS), offers a means to gather information on road quality without the need for large-scale field measurements. The development of a methodology for determining the trafficability of forest roads, based on road characteristics derived from remote sensing data, would provide an accessible approach, eliminating the need for specialized expertise.

The condition of forest roads has been determined in the past using various remote sensing methods. In particular, dense-pulse airborne Light Detection and Ranging (LiDAR) data has shown a potential for use in determining road quality and width as well as identifying centerlines and curves that are too steep for semi-trailer trucks (Azizi et al. 2014; Craven and Wing 2014; Waga et al. 2015; Waga et al. 2021; Karjalainen et al. 2024). Similar results regarding the steepness of curves have also been obtained using coarser flight laser data. Ferraz et al. (2016), Hruza et al. (2018) and Waga et al. (2016), studied four methods for observing the quality of a road surface: Airborne laser scanning (ALS), Mobile Laser Scanning (MLS), Terrain Laser Scanning (TLS), and Close-Range Photogrammetry (CRP). MLS is widely used in urban areas to scan pavements and paved roads in order to assess their quality and maintenance needs, while Hruza et al. (2018) found that Terrain Laser Scanning is also an efficient method for detecting possible defects in a road surface. The National Land Survey of Finland provides exciting sparse ALS data (0.5 points/m^2) for the whole area of Finland (gathered in 2008 – 2019) (National Land Survey of Finland 2021a) and started gathering denser ALS data (5 points/m^2) (National Land Survey of Finland 2021b) in 2020. When using sparse ALS (0.5 p), a dense canopy cover can greatly reduce the detection of roads. However, the 5-point ALS data is dense enough to offer precise information regarding numerous road properties regardless of canopy cover. The new ALS database covers the whole of Finland and will play a pivotal role in the future modeling and assessment of forest roads.

In addition to laser scanning methodologies, alternative approaches have demonstrated promise in the evaluation of forest road quality. Peng et al. (2021) conducted research on the use of satellite radar interpretation for the monitoring of soil moisture over large areas, providing cost-efficient and high frequency data. The method would be ideal for monitoring dynamic road conditions and trafficability based on changes in surrounding terrain moisture. Aleadelat et al. (2017) studied the effectiveness of employing Android-based smartphones in the estimation of ride quality on gravel roads. Their findings yielded promising results, suggesting the potential for a cost-effective crowdsourcing approach that could be highly advantageous when considering the inventories of private forest roads.

Research on the trafficability of forest roads, whether through manual measurements or the collection of data using ground-based mobile devices (see Dapeng and Li 2021; Heidari et al. 2022), is laborious due to the need of collecting data directly from the field. Despite the rapid fluctuations in the conditions of gravel roads (Selim and Skorseth, 2000), it is not economically feasible to repeatedly observe/measure/review more than a subset of selected forest roads, given the labour required to collect the data. Furthermore, techniques such as the recording of vibration using an accelerometer must be carried out in a standardised manner that takes into account all influencing factors to ensure consistent results. These factors may include driving speed, vehicle suspension, arrangement of the measurement device sensors, as well as the sensor types.

1.6 Gamma-ray spectrometry and trafficability estimation

Gamma-ray spectrometry measures the gamma radiation emitted from the natural decay of radioactive elements present in soil material (Cook et al. 1996). Although there are many naturally occurring radioisotopes, only three elements, potassium (%K), uranium (ppm eU) and thorium (ppm eTh), have isotopes that emit gamma radiation with sufficient intensity to be measured at airborne heights (Minty, 1997). The energy intensity of these elements ranges 1.37–1.57 MeV for potassium, 1.66–1.86 MeV for uranium and 2.41–2.81 MeV for thorium. Each rock and sediment typology has a typical amount of these radionuclides, which results the gamma-ray spectra and allows us to detect different soil and rock types (Priori et.al. 2014).

Gamma rays can penetrate up to 30 cm of rock and 50 cm of soil, and several hundred metres of air, and therefore these are the only choice available for the remote sensing of terrestrial radioactivity (Grasty, 1997; Minty, 1997). The technique has been used for soil survey for over 30 years. It has been stated by several authors (Grasty, 1997; Hyvönen et al. 2003) that gamma radiation decreases in intensity with increasing soil moisture and that the soil moisture content is one of the most important factors that can be utilized for the classification of soil material and soil types (Schwarzer, 1973; Lundien, 1976; Pohjankukka et al. 2014). Gamma-ray spectrometry data have also been used in several studies to detect different soil attributes e.g., clay, silt, and organic carbon (Heiskanen et al. 2020; Taylor et al., 2002; Wong and Harper 1999), soil pH (Dierke and Werban, 2013; Wong and Harper, 1999), and soil stoniness (Priori et.al. 2014; Heiskanen et.al. 2020). Vegetation not only attenuates the gamma radiation but also acts as a competing source of it, although the concentration of radioactive elements in vegetation is only a fraction of that in the bedrock and soil. In boreal forests, consisting mostly of pine and/or spruce-dominated stands, the concentration of radioactive elements in the forest biomass is marginal compared with that in the underlying soil (Kogan et al. 1971).

The radiometric fingerprint of a site mainly depends on the parent material, its mineralogy and geochemistry (Dickson and Scott, 1997). In general, the radiometric fingerprint of the parent material is inherited to the soils which develop from them. However, the soil formation process can also alter the nuclide signature of soils through hydrolysis, protolysis and redistribution of soil material by erosion process (Taylor et al. 2002; Herrmann et al. 2010). The radiometric signal varies across landscapes and it reacts to different patterns in the terrain which indicate variation in soil properties, but the application does have several limitations (Marchuk and Ostendorf, 2009). The use of gamma radiometrics for soil proximal sensing is strongly site specific, because of the influence of parent material mineralogy on the gamma-rays emitted from the soil (Priori et.al. 2014). In addition, the data gathered using airborne gamma-ray acquisition systems often have poor spatial resolution for small-scale applications (Marchuk and Ostendorf, 2009; Wilford and Minty, 2007).

Hand-held gamma-ray sensors have been used in geological studies (Moskalewicz et al. 2022; Sandersson et al. 2002; Kock and Samuelsson, 2011) and can be used to obtain location-specific data. These instruments are often used for soil studies and provide much better spatial accuracy than low-resolution airborne gamma-ray data.

The intensity and energy distribution of gamma-ray emissions are influenced by various factors, including the abundance of radioactive isotopes, soil moisture content, and soil density. The gamma-ray data offers information about soil composition, mineralogy, and geological structures, which are essential for terrain trafficability estimation, by providing insights into soil composition and moisture content, helping us identify areas with favorable

or unfavorable terrain conditions for forest machinery. For example, high concentrations of clay minerals or organic matter detected by gamma-ray spectrometry indicate areas with low bearing capacity and soil compaction. The resolution of airborne gamma-ray detectors may be insufficient to capture fine-scale variations in soil properties, especially in heterogeneous terrain. In addition, natural variations in background radiation levels and environmental factors, such as vegetation cover and topography, can complicate data interpretation and analysis. Integration with other remote sensing techniques, such as LiDAR and hyperspectral imaging, can provide complementary information about terrain characteristics and enhance the accuracy of trafficability assessments.

1.7 Objectives

The overall objective of the thesis was to determine how well the characteristics affecting terrain and forest road trafficability can be evaluated using openly available information and data. In terms of terrain trafficability, we focused on soil stoniness, soil depth and peat depth predictions. For the prediction of forest road trafficability, we aimed to use properties that are already openly available or can be derived from sufficiently dense ALS data. We also introduced the use of gamma-ray spectrometry as a part of the road bearing capacity predictions. The specific aims of the respective studies were as follows:

I: To evaluate whether the stoniness of the topsoil could be predicted using gamma-ray values from low-flying geophysical data combined with soil type information, both of which are available as open-source data in Finland. The gamma-ray values and soil type were studied using regression analysis and compared with measured stoniness index reference data.

II: To evaluate which characteristics of forest roads and the surrounding terrain could be used to predict their bearing capacity and overall trafficability, and if any type of gamma radiation (U, Th, K) was sensitive to road bearing capacity. The bearing capacity data was collected with single-time measurements. The research was carried out by analyzing the collected forest road properties, LFWD and gamma-ray measurements using linear mixed-effects models.

III: To compare two gamma-ray spectrometry datasets, which were acquired from the same sample plots but measured with different methods. The dataset for the first method was collected using airborne gamma-ray spectrometry and the dataset for the second method was collected with a handheld gamma-ray spectrometer. This study had two sub-objectives:

(1) To determine whether there was a significant relationship between the gamma-ray datasets, and if so, whether the gamma values collected with the handheld device could be derived from the airborne gamma data.

(2) To study the individual performance of the datasets when predicting topsoil stoniness, mineral soil depth, and peat depth. We wanted to assess whether there was a significant difference in the prediction accuracy of the datasets and if so, which dataset offered the better prediction results.

2 MATERIALS AND METHODS

2.1 Study areas and plot design

The research was carried out in two study areas located in the regions of North Karelia, North Savonia, and South Savonia in Eastern Finland (Fig. 1). The forests of the study areas are mostly dominated by Scots pine or Norway spruce, with deciduous trees found in minor proportions. The soil type in the study area is either peat or mineral soil (till and moraine mainly composed of granite and gneiss), since the majority of the fine-grained mineral soils (silt and clay mixtures) are in agricultural use.

Field data used in studies **I** and **III** were collected from study area I **(**Fig. 1**)**. The collected field data consisted of terrain characteristics measurements (described later) and handheld gamma-ray spectrometer measurements which were measured separately from terrain characteristics. The terrain characteristics measurements were used in both studies **I** and **III** but handheld gamma-ray spectrometer measurements were used only in study **III**. Both studies use also airborne radiometric data which was acquired from Geological Survey of Finland.

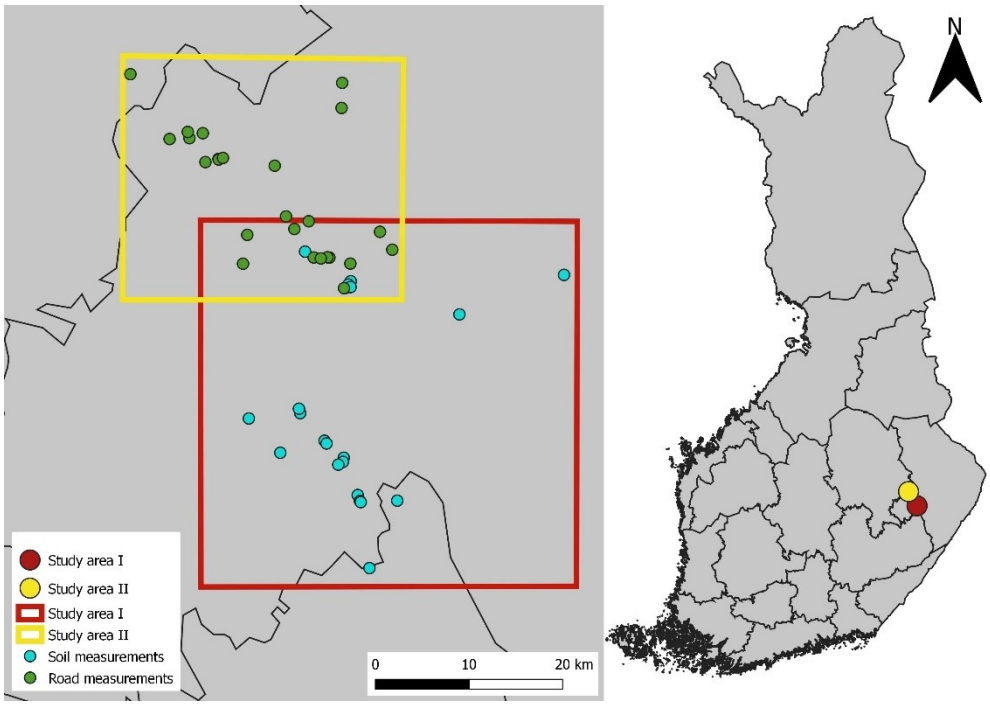

Figure 1. Locations of the study area I (studies **I** and **III)** and study area II (study **II**). Coordinates of study area of study area I: Northwestern corner 62°39’56”N 28°48’41”E; southeastern corner 62°18’7”N 29°33’52”E (WGS84, EPSG:4326). Coordinates of study area II: Northwestern corner 62°49’27”N 28°39’30”E; southeastern corner 62°34’57”N 29°13’28”E (WGS84, EPSG:4326).

The field data for study **II** was collected from the study area II (Fig. 1) which partially overlaps the study area I**.** The field data consisted of measurements of different forest road characteristics (described later) as well as hand-held gamma-ray spectrometer measurements on the same roads.

2.2 Data collection for studies I and III

2.2.1 Field measurements

The overall soil characteristics data were collected in the summer of 2017 from 69 clear-cut sites that varied in size from 0.15 hectares to 6.3 hectares. The sample plots were arranged in an even grid and both the number of plots and the distance between sample plots were proportional to the size of the clear-cut area, so that each site was evenly measured. A total of 1221 sample plots were measured from these clear-cut areas, 828 with mineral soils and 393 with peatland. The location of each plot was determined using a high precision GPS device. The coordinates of the sample plots were post-corrected and the locations saved as a point-type shapefile.

The study sites varied across the measured variables and the site characteristics. The majority of the study sites containing the measured plots were non-drained mineral soils that are characterized by dryness and contain little organic matter. Some sites were more wet boggy mineral soils having a shallow peat layer (depth less than 30 cm) on top of the mineral soil. The majority of these sites were drained (drained mineral soil). The presence of these mixed soil sites is due to the fact that the sites were planned for forestry operations (clearcut areas), so the boundaries were determined according to tree species rather than soil characteristics. The topography of the mixed soil sites was relatively flat with gentle slopes. Mineral soil mounds were common, especially at the drained mineral soil sites (visible in Fig. 2). The non-drained mineral soil sites varied in topography from flat to rough, steeper slopes.

All of the measured sample plots were assessed with respect to the stoniness of the topsoil, topsoil type, as well as soil and peat depth. These parameters were assessed by utilizing a ground spike, a tool designed for precise soil measurement. For mineral soils, the soil type was assessed by visual estimation from a soil sample extracted from the top 30 centimeters of the sample plot. The soil type was confirmed for a number of plots using an open-source soil map (Geological Survey of Finland 2023). The soil types identified in studies **I** and **III** were peat, fine-till, sandy-till, and sand.

The stoniness of the topsoil is expressed here in terms of the Stoniness Index (SI), which describes the stone content at depths of 20–30 centimeters (Melander et al. 2019). The determination of stoniness in the topsoil was carried out using the soil surface penetration method (Viro's method), where a ground spike was inserted into the soil within the designated sample plot to a depth of 20–30 centimeters, and the number of stone contacts was counted (Viro, 1952). The stoniness was measured by making 10 insertions 1 meter apart along the line of sample plots and increasing the index for that plot for each contact with a stone, resulting in a Stoniness Index (SI) of 0–10, e.g. zero contacts = SI 0, one contact = SI 1, two contacts = SI 2, etc. No attempt was made to avoid stones visible on the ground surface. The SI values were classified into Stoniness Index Classes (SIC) ranging from 1 to 5 (in study **I**) and 1 to 3 (in study **III**). This was carried out after it was determined that a small variation in stoniness (SI values) would not be significant as far as forest operations or the bearing

capacity of the forest soil were concerned. The distribution of the SI and SIC (1-5) values is shown in Table 1. It is the SIC values that will be used as the key criteria here when assessing the models and analyses.

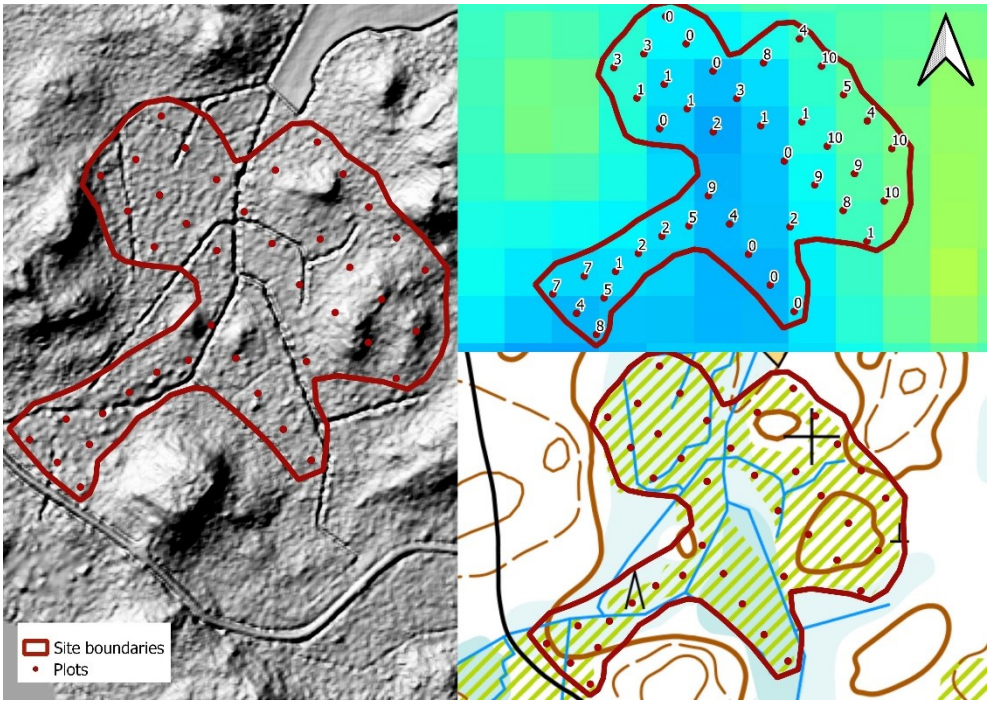

Figure 2. The radiometric components measured A map illustrating the measured plots within one stand (selected from a total of 69) from the original dataset. The map in the top-right corner presents the gamma radiation map of potassium as raster data with a pixel resolution of 50 meters (Geological Survey of Finland 2023). The numerical values indicate the Stoniness Index (SI) for each measured plot and are shown only on the top-right corner map. The map on the left depicts the study site using a Hillshade digital elevation Model (DEM) with a 2-meter pixel resolution as the basemap (National Land Survey of Finland 2024). The map in the bottom-right corner displays the site overlaid with a topographical map, where blue areas denote peat soil, and white areas represent mineral soil (National Land Survey of Finland 2024). The predominant soil type on the stand is peat, with occasional mounds of mineral soil, which are visible on both the hillshade and topographical maps. Coordinates at the center of the site 62° 36'3"N 29°7'21"E (WGS84, EPSG:4326).

The mineral soil and peat depth measurements were taken in the center of each sample plot, and each measurement was assigned to one of three categories: < 30 cm, 30–60 cm or > 60 cm. For mineral soils, the depth was determined when the ground spike made contact with bedrock or a large underground boulder. For peat soils, the depth of the peat layer was determined when the ground spike encountered subsoil or bedrock. To account for the

possibility that the ground spike coincidentally hit a small rock on the first penetration, the measurements were taken at several locations within the sample plot.

Table 1. Deviation of stoniness index (SI) and stoniness index classes (SICs) and soil types in the sample plots of study **I**.

			Potassium (K)			Thorium (Th)			Uranium (U)		
		N (%)	Min	Max	Mean	Min	Max	Mean	Min	Max	Mean
SI	0	70 (27.45)	-2.99	0.55	-0.88	-3.07	1.43	-0.75	-2.41	1.58	-0.59
	1	9 (3.53)	-2.85	0.33	-1.07	-1.95	0.89	-0.66	-1.23	1.06	-0.28
	2	7 (2.75)	-1.60	1.52	-0.22	-1.71	1.67	0.09	-1.78	0.30	-0.56
	3	10 (3.92)	-1.15	1.53	0.37	-1.29	1.46	-0.04	-0.66	0.27	-0.17
	4	16 (6.27)	-0.96	1.82	-0.04	-0.95	1.24	-0.20	-1.48	1.53	-0.37
	5	18 (7.06)	-1.44	1.58	0.40	-1.40	1.67	0.30	-2.32	1.33	-0.06
	6	21 (8.24)	-0.96	1.11	0.20	-1.00	1.16	0.24	-1.45	1.39	0.21
	7	31 (12.16)	-1.43	2.05	0.36	-1.31	2.39	0.43	-1.32	2.37	0.28
	8	30 (11.76)	-1.19	1.86	0.48	-1.40	1.88	0.40	-1.04	2.12	0.35
	9	20 (7.84)	-0.25	1.51	0.71	-0.61	1.62	0.34	-1.09	2.30	0.63
	10	23 (9.02)	-0.25	1.65	0.72	-0.93	3.51	0.73	-1.07	3.02	0.76
SIC	1	79 (30.98)	-2.99	0.55	-0.92	-3.07	1.43	-0.74	-2.41	1.58	-0.56
	2	17 (6.67)	-1.60	1.53	0.11	-1.71	1.67	-0.13	-1.78	0.30	-0.39
	3	55 (21.57)	-1.44	1.82	0.17	-1.40	1.67	0.14	-2.32	1.53	-0.03
	4	61 (23.92)	-1.43	2.05	0.47	-1.40	2.39	0.46	-1.32	2.37	0.36
	5	43 (16.86)	-0.25	1.65	0.76	-0.93	3.51	0.59	-1.09	3.02	0.71
Peatland		77 (30.20)	-2.99	1.82	-0.77	-3.07	1.43	-0.74	-2.41	2.37	-0.53
Fine till		19 (7.45)	-1.07	0.27	-0.50	-0.73	0.45	-0.22	-1.04	0.20	-0.11
Sandy till		141 (55.29)	-1.43	2.05	0.49	-1.31	2.39	0.38	-1.48	2.30	0.29
Sand		18 (7.06)	-1.44	1.95	0.00	-1.40	3.51	0.40	-2.32	3.02	0.07

2.2.2 Gamma- ray data and the sampling of datasets

The airborne radiometric data were acquired from the national low-flying geophysical database maintained by the Geological Survey of Finland (GSF). The low-altitude surveys in question were conducted from 1972 to 2007, by which time the database covered the whole of Finland. The geophysical parameters measured included the Earth's magnetic field, the electromagnetic field of the Earth's crust and natural gamma radiation (radiometric). However, the present studies focus exclusively on the gamma-ray data, which comprises

measurements of natural gamma-ray radiation, potassium (%K), uranium (ppm eU), and thorium (ppm eTh), emitted from the ground (Hyvönen et al., 2005).

The ground speed of the aircraft during the measurements was approximately 50 meters per second, and the flight altitude ranged from 30 and 40 meters. The radiometric measurements were performed for positions approximately 40 meters apart along flight lines, usually located at 200-meter intervals. The gamma radiation data covering the research area was measured in 1981 and 1991. The gamma-ray spectrometer employed in the surveys used a scintillation detector with a 25 liter NaI(Tl) crystal. The radiometric components measured were interpolated into pixels 50 meters in size (Fig. 2).

For the training dataset of study **I,** all the fine-grained mineral soil (fine-till) plots were included in the dataset, and mineral soil, as well as peatland plots were selected using a sampling approach. The sampling was carried out by including those plots that were close enough to the GSF's low-flying geophysical data flight lines for which the data is available from the GSF's open data site (Hakku.fi). The flight lines were buffered with 20-meter zones on both sides of the flight line, resulting in a buffer zone with a total width of 40 meters. Plots that were outside the buffer zones were excluded from the original dataset. This was done because, although the distance between the flight lines was approximately 200 meters, the actual measurement zone was only 40 meters wide, thus leaving a distance of approximately 160 meters between the flight lines with no direct measurement. Therefore, the process acquired radiometric values that were not the result of interpolation. The sampling process reduced the number of plots from 1,221 to 255 (Dataset 1). For the selected plots the values of each gamma component were extracted from the gamma radiation data which consisted of three raster format files, each containing the values of one gamma radiation component, i.e., potassium (K), uranium (U), thorium (Th). For study **I**, a second dataset (Dataset 2) was also selected, consisting solely of mineral soil plots. The sampling of Dataset 2 was carried out manually in such manner that all the SIC classes were evenly represented. A total of 215 plots were selected for study **I** and subsequently divided into subgroups for the training and testing of the predictive model.

For study **III,** a second field measurement campaign was conducted in July 2020, where 145 plots were manually selected from the original dataset (n = 1,221) to ensure representation of variations in soil/peat depth and stoniness, thereby creating a balanced dataset regarding soil properties (Table 2). The selected plots were then assessed for their natural gamma radiation levels. The gamma-ray values were collected by taking a single measurement from the center of each plot. The gamma-ray measurements were carried out using a Georadis GT-40 (Fig. 3) with a 3 × 3" NaI/Tl detector, which is a portable/handheld multifunction gamma-ray spectrometer. The GT-40 unit utilizes a 1024 channel linear energy spectrometer and pile-up rejection with built-in continuous analysis (Georadis, 2023). The unit uses automatic stabilization based on natural background radiation during the operation, eliminating the need for additional radioactive sampling (Georadis, 2023). The selected plots were assessed with respect to their potassium (%K), uranium (ppm eU), and thorium (ppm eTh) values. This resulted in two separate gamma-ray datasets for each plot.

2.3 Data collection for study II

For study **II**, the field data were collected in the autumn of 2022. The data were measured from 25 forest roads, totaling 113 sample plots, which were arranged at regular intervals of 25 meters and ranging from 3 to 5 per road segment. The measurements were conducted on

a single point per plot in the middle of every 25-meter segment. The roads for the measurements were selected manually, with the objective of finding roads that varied in their constructional properties and surrounding terrain characteristics. The primary tool used for the selection of the roads to be measured was to use soil type vector maps by the Geological Survey of Finland (Geological Survey of Finland, 2024), at scales of 1:20 000/1:50 000 which were used to identify variation in soil types surrounding the roads.

The forest roads within the study area are primarily owned by private road maintenance associations which include private road owners, forest companies, and Metsähallitus, a state-owned entity responsible for the management of state forests. The forests in the area are in active use for forestry purposes and by individuals. The selected roads vary in size, with larger roads utilized throughout the year by various parties (transportation companies, forestry, individuals, etc.), and smaller dead-end roads, which often lead to forest operation sites and are not used as frequently, and are often not accessible all year round.

The majority of the selected road sections were located on mineral soils and a minor part of the roads were built on drained peatlands. The selected road sections were assessed through field measurements of roadway width, usable road area, and ditch depth. Site attributes such as habitat type and soil type were also determined for each plot, mainly through an open-source website (Geological Survey of Finland 2024). If there was uncertainty about the surrounding soil type, it was assessed by eye from a sample taken from the terrain surrounding the road at the location of the sample plot.

Table 2. Deviation of soil types, SICs, soil depth, and peat depth on air gamma and ground gamma in the sample plots of study **III**

				Air gamma mean			Ground gamma mean		
		N	%	K	Th	U	K	Th	U
	Peatland	60	0.41	-0.64	-0.41	-0.71	-0.82	-0.77	-0.84
	Fine-grained till	15	0.10	-0.35	-0.21	-0.18	-0.24	-0.22	-0.28
	Sandy till	55	0.38	0.96	0.74	0.91	0.53	0.61	0.69
	Sand	15	0.10	-0.98	-1.08	-0.47	0.45	0.23	0.67
SIC	1	66	0.46	-0.59	-0.32	-0.53	-0.67	-0.59	-0.75
	2	41	0.28	0.34	0.17	0.28	0.18	0.07	0.25
	3	38	0.26	0.52	0.28	0.54	0.52	0.63	0.85
Mineral soil depth	< 30cm	17	0.20	1.06	0.82	0.86	0.85	0.76	1.21
	30 - 60 cm	22	0.26	0.70	0.55	0.85	0.46	0.48	0.69
	> 60cm	46	0.54	-0.01	-0.10	0.14	0.16	0.23	0.17
Peat depth	< 30cm	20	0.33	-0.35	-0.26	-0.61	-0.35	-0.53	-0.28
	30 - 60 cm	20	0.33	-0.49	0.15	-0.68	-0.87	-0.71	-0.67
	> 60cm	20	0.33	-1.09	-1.11	-0.85	-1.24	-1.06	-1.57

Figure 3. Hand-held gamma-ray spectrometer on the left and Light falling-weight deflectometer (LFWD) on the right.

2.3.1 Measured road characteristics

The width of the roadway (RW) was measured with a tape measure to an accuracy of 10 centimeters. For this purpose, the roadway was defined as the distance between the outer borders of the ruts made by the vehicle tires. If the ruts of the roadway were not at all detectable, the same measurement as useable road width (URW) was used. The width of the useable road surface (URW) was measured similarly, with the same level of accuracy as RW. The measurement of URW consisted of the total width of road surface useable by vehicles. Several factors affected how this useable road width was measured. If there was a clear crushed rock layer (continuous bed of crushed rock particles sized 30 – 60 mm) on the road, the width of this layer was measured. Usually on forest roads there are different sizes of particles on the road surface but lacked a clearly defined crushed rock layer. If there was no crushed rock layer visible on the road surface, then the width between ditches was measured, and if there was clearly softer area closer to the ditches this area was excluded from measurement. If the road segment did not have ditches, then the distance was measured where the road surface clearly changed into the surrounding terrain.

The depths of the ditches on both sides of the road, i.e., the vertical distance between the bottom of the ditch and the level of the road surface, were measured to an accuracy of 5 centimeters using a tape measure. If a measurement fell between two five-centimeter segments, the result was rounded down. If the road embankment descended directly into the terrain, the depth was marked as “x” to be processed later. The depths in these cases were later converted into a depth of 200 cm.

2.3.2 Falling weight and gamma-ray measurements

During October and November 2022, the same roads/plots were then measured with a Light Falling Weight Deflectometer (LFWD) (Fig. 3) to determine their surface stiffness and bearing capacity (MN/m^2). The LFWD unit was built by a company named Terratest GmbH (Terratest, 2022). A period of heavy rainfall preceded the measurements, so the road structures were saturated. In order to obtain the most realistic bearing capacity values possible, the falling weight deflectometer measurements were performed on the wheel paths of the road, where the road material is compacted by the passage of vehicles. A total of two measurements were taken on each plot from both wheel paths. The Light Falling Weight Deflectometer (LFWD) is commonly used to evaluate the physical properties of paved and unpaved roads by estimating the structural capacity to determine their overall quality and to detect any weak points in their surface structure (George, 2003; Kaakkurivaara et al. 2015). The lightweight falling weight deflectometer mimics the wheel load of a truck using an impulse method, where a load plate is placed on the road surface and then a mass is dropped onto the plate. The force of the falling mass is transferred through the plate to the surface, causing a deflection that is measured and then converted to load bearing capacity values (MN/m^2) through a computational procedure (Saarenketo and Aho 2005, Kaakurivaara et al. 2015).

The same plots were measured using a handheld gamma-ray spectrometer (same as in study **III**). The gamma-ray measurements were taken simultaneously with the LFWD measurements, and they were taken from exactly the same points. So, two gamma-ray measurements were conducted on each plot from both wheel paths of the roadway. This way we could safely assume that these two data are directly comparable since both were measured during the same levels of moisture in the road.

Upon closer examination of the data, we noticed an outlier in the LFWD measurements that was nearly three times higher than any other measurement on that particular road section, and it occurred only on the left tire track of the roadway. We believe that it was caused by a rock which was close to the road surface. The exceptionally high LFWD value was deemed to exist due to measurement error or an abnormality on the road and was therefore excluded from the final dataset, thus reducing it to n=111. (Table 3)

2.3.3 Depth-to-water index

Depth-to-Water (DTW) data (Salmivaara, 2020) were acquired from the Natural Resources Institute of Finland (Open download service Paituli.csc.fi). The calculation of the DTW moisture index (Murphy et al. 2007, 2008, 2009) has been made based on the National Land Survey's 2-meter digital elevation model (DEM) (National Land Survey of Finland, 2019). DTW is based entirely on DEM, so soil type information or weather conditions are not taken into account, and this causes slight uncertainty (Ågren et al. 2014; Lidberg et al. 2020). DTW maps have been created with 4 thresholds, representing different hydrological conditions, i.e., that calculated with a 0.5 ha threshold represents extremely moist conditions (after the snow has melted), that with a 1 ha threshold represents moist conditions, that with a 4 ha threshold dry conditions, e.g. at the end of summer, and that with a 10 ha very dry conditions (Ågren et al. 2014). DTW values were extracted for each plot from the DTW maps by creating a buffer zone with a radius of 12.5 meters around every plot and calculating an average DTW value from the values inside the buffer zone (Table 3).

Table 3. Summary statistics (mean, standard deviation, minimum, and maximum) on the used variables in dataset (n=111) for study **II**. Soil types have their amount reported as count (N) and percentage (%) on how many plots that soil type has occurred. Min. and Max. tell how many plots there was on a single road with that soil type.

	Mean	SD	Min.	Max.
Number of plots measured/Road (Plots)	4.44	0.80	3.00	5.00
Roadway width (RW)	272.25	45.75	200.00	380.00
Useable road width (URW)	359.01	85.29	250.00	570.00
Depth-to-water index (DTW)	571.32	384.71	77.74	1771.90
Ditch index (DI)	56.37	49.93	0.00	200.00
Light Falling-weight deflectometer value (LFWD)	39.59	17.20	6.60	77.45
Potassium (K)	2.02	0.23	0.53	0.79
Thorium (Th)	6.23	1.41	1.03	3.98
Uranium (U)	2.07	2.48	3.41	8.32
Soil type	N	%	Min.	Max.
Peat	24	21.62	0	5
Fine-grained till (FT)	14	12.61	0	5
Sandy till (ST)	54	48.65	0	5
Sand	19	17.12	0	5

2.4 Data characterization

In all studies (**I-III**) the gamma-ray data used, (both airborne and handheld gamma spectrometer measurements) were normalized using z score normalization (Eq. 1), which scales the values in relation to the mean of the population.

$$X_{norm} = \frac{X_i - X_{mean}}{S} \quad (1)$$

where x_{norm} is the normalized value of the gamma component, x_{mean} is the mean for the population and S is the standard deviation within the population.

In study **II** a Ditch index (DI) was calculated which is a mean of the ditch depths on a single plot (Eq. 2) It describes how well the drainage works and whether the ditches are deep enough to keep the water away from the vicinity of the road structure.

$$DI = \frac{(D_L + D_R)}{2}\ , \quad (2)$$

where DI is the Ditch index, D_L is the left-side ditch depth, D_R is the right-side ditch depth. The higher the Ditch index, the better was the overall ability directing water away from the vicinity of the road structure. If during field measurements a ditch depth was marked as "x" it was converted to a depth of 200 centimeters because it was seen that these steep descends

have a similar effect as high quality ditches. In study **II** the soil information was transformed into soil coefficients according to the table presented in the study Suvinen (2006). These coefficients represent the rolling resistance of the soil.

Correlation coefficients were calculated for each study to detect high correlations among independent variables to highlight a possible risk of multicollinearity which was then further tested using a variance inflation factor test (VIF) (Kuhn et al. 2020). In study **III** ANOVA test (analysis of variance) was conducted to investigate whether the mean values of each gamma component (air gamma and ground gamma) varied significantly between SIC and soil/peat depths.

Commonly boxplots were utilized in all of the studies (**I-III**) to visually observe the relationships of important variables of the datasets. In study **I** boxplots were used to observe the relationships between stoniness (SI and SIC) and the normalized airborne gamma-ray values. This analysis was conducted on both the complete dataset (Dataset 1) and a dataset limited to mineral soil data (Dataset 2) (Fig. 12). In study **II** the boxplots were created to observe the relationships of Light Falling weight measurement values (LFWD) (MN/m^2) and usable road width and soil types. Similarly, boxplots were created for soil types and DTW and Ditch index to study whether ditch depth in our data depends on the surrounding soil type on which the road is built (Fig. 5). In study **II** a normal scatter plot was also used to detect the relationship between handheld gamma-ray measurements and LFWD values (Fig. 6). In study **III** similar boxplots to study **I** was created where we observed the relationship between SIC values and both normalized airborne gamma and ground gamma **(**Fig. 13**).** In study **III** boxplots were also created to investigate the relations of mineral soil and peat depths to these same gamma values **(**Fig. 8 and 9**)**

2.5 Data analysis

2.5.1 K-fold ordinal regression

In study **I** the main method used in the analytical modelling was ordinal regression since both SI and SIC were class form variables, i.e., the predicted values were selected through class probability. Ordinal regression is commonly used to predict the behaviour of level-dependent variables, since the dependent variable is assumed to be consecutive, and each level must be in an ordered scale. Ordinal regression was used to determine the significant independent variables to be used in the final models, and K-fold cross-validation was used when constructing each model by means of 10 folds and three repeats. The main goal was to determine whether the stoniness of the topsoil (SI and SIC) can be reliably predicted using gamma radiation data and soil type information, and to construct a model for this that could be based on openly available geographic information. A total of three ordinal regression models were constructed to predict SI and SIC. Ordinal regression was performed first on the SI for Dataset 1, taking both gamma radiation values and soil type dummy variables as predictors. Secondly, we constructed a similar model but replacing SI with SIC, and thirdly, we constructed another SIC model using Dataset 2 with only gamma-ray values as predictors to see how well these values performed with respect to mineral soil stoniness alone.

Ordinal regression does not give us a class estimate directly, but instead the result is a plot-specific y-value (Eq. 3), so that a class pair probability can be calculated for each plot by comparing this y-value with a plot-specific z-value (Eq. 4). We can then further calculate the class-specific probabilities (Eq. 5 – 9) and choose the class with the highest probability.

An ordinal regression model is relatively laborious to use compared with regular linear regression precisely because of these class probability calculations.

$$y = \boldsymbol{\beta}_i \mathbf{X}_i \ldots + \varepsilon_i \quad (3)$$

where y is a plot-specific y-value, $\boldsymbol{\beta}$ is the regression coefficient for the predictor variable $\boldsymbol{X}$ and $\boldsymbol{\varepsilon}$ is a random error term.

$$p_x = \frac{1}{1+e^{-(z_x - y)}} \quad (4)$$

where p is the class pair probability (1:2; 2:3; 3:4; 4:5), z is the class pair-specific z-value provides by the ordinal regression analysis, and y is the y-value acquired from Eq. 3. We were able to derive a class-specific probability value $p_1 - p_5$ (Eq. 5 – 9) from the class pair probability p:

$$p_1 = p_{1\ or\ 2} \quad (5)$$
$$p_2 = p_{2\ or\ 3} - p_1 \quad (6)$$
$$p_3 = p_{3\ or\ 4} - p_{2\ or\ 3} \quad (7)$$
$$p_4 = p_{3\ or\ 4} - p_{4\ or\ 5} \quad (8)$$
$$p_5 = 1 - p_{4\ or\ 5} \quad (9)$$

where p_1 is the probability of class 1, p_2 is the probability of class 2, p_3 is the probability of class 3, p_4 is the probability of class 4 and p_5 is the probability of class 5.

The key assumption in ordinal regression is called assumption of proportional odds which assumes that the independent variables have the same effect on the odds across all levels of categories/classes (i.e., relationship between each class-pair is the same). Since our models estimate one equation over all levels of SI or SIC, we conducted the test of parallel lines for each of our models to see whether the assumption of proportional odds holds. Test of parallel lines compares our ordinal model which has one set of coefficients for all class-pairs, to a new model with a set of class pair-specific coefficients. If the model with separate coefficients for every class pair gives significantly better fit to the data, we reject the assumption of proportional odds.

2.5.2 Linear mixed effects models

The main analysis method used to predict the LFWD values from forest roads in study **II** was Linear mixed effects models (LME). Linear models (regression models) have been commonly used in the field of forestry especially in the prediction of forest attributes with ALS metrics. However, the data often have a grouped structure as for example in our case many observations are measured within one road section and it is safe to assume that two observations within one road section are more alike than two observations from different road sections. The variance-covariance structure between observations affects the standard errors of the estimated regression coefficients, so ignoring within group correlations in the model construction phase may lead to severe problems in parameter estimates and model inference (Mehtätalo and Lappi, 2020). Therefore, instead of regular linear models that are fitted with the ordinary least squares method and the assumption that the residuals are uncorrelated, linear-mixed effects models should be used to take the correlation structure into account.

In LME models, the group effects are modelled as random variables, i.e. the group effects are the same for all members within the group and are different between members of different groups. There can be one or more random effects in a mixed-effect model. In this thesis, a total of three LMEs were constructed. The general form of each of the models is shown in Eq. 10.

$$\boldsymbol{y}_{ki} = \boldsymbol{X}_{ki}\boldsymbol{\beta} + \boldsymbol{u}_k + \boldsymbol{\varepsilon}_{ki} \quad (10)$$

where $\boldsymbol{X}_{ki}$ is the vector of fixed predictor variables for plot i on road k, $\boldsymbol{\beta}$ is a vector including regression coefficients for the fixed effects, $\boldsymbol{u}_k$ is the random effect for road k, and $\boldsymbol{\varepsilon}_{ki}$ is the residual error for plot i on road k.

The first of three LME models with LFWD as response variable was constructed using stepwise selection of most significant variables (LME-1). For the second model (LME-2) it was decided to include gamma-values in addition to road characteristics to the model even though they would not reach significance. Third model (LME-3) was constructed since one variable in our set of predictors was overpowering every other variable, thereby dropping them from the model. Thus, the third model (LME-3) was constructed to see how big of an effect the overpowering variable has in the resulting statistics. Homoscedasticity of residuals was evaluated in the selection of the final predictors using VIF test.

2.5.3 Linear discriminant analysis

The linear discriminant analysis (LDA) was used as the main method in study **III** where we predicted the SICs and mineral soil and peat depths. The main objective of linear discriminant analysis is to find a linear combination of features that best separates different classes in the data. It aims to maximize the separation between classes while minimizing the variation within each class. LDA does this by projecting data with two or more dimensions into one dimension so that it can be more easily classified. The technique is, therefore, sometimes referred to as dimensionality reduction. Linear discriminant analysis assumes that the features within each class are assumed to follow a multivariate normal distribution, and that the decision boundaries between classes are assumed to be linear. Once the linear discriminants are computed, they can be used to classify new observations into different classes. This is done by evaluating the discriminant functions for each class and assigning the observation to the class with the highest discriminant score.

Category = f(Air K, Air U, Air Th; Ground K, Ground U, Ground Th | soil type)

where

Category	*Topsoil stoniness (SIC) or soil/peat depth*
Air *	*Airborne gamma-ray response for potassium, uranium and thorium*
Ground *	*Ground gamma-ray response for potassium, uranium and thorium*
soil type	*Categories from soil map (fine-till, sandy-till, and sand)*

2.6 Validation of models and accuracy assessment

In study **I** the accuracy of the SI and SIC models (Dataset 1) was further tested by performing a classification of 500 randomly selected sample plots from the initial complete data

(n=1,221). The accuracy of the second SIC model (only mineral soil) was tested by dividing the dataset 2 into training and testing datasets in a ratio of 0.7:0.3. In studies **II** and **III** to avoid overly optimistic results, Leave-one-out cross-validation (LOOCV) was used. In LOOCV, the predictions are always produced by excluding the observation in question from the training data and, possibly the observations from the same group as well (e.g. from the same road).

The accuracies of stoniness (SI and SIC) classification results in studies **I** and **III** were assessed using cross-tabulations of the predicted and observed SI and SIC values. The main key statistics in the accuracy assessments were the percentage of agreement and the Kappa value (Eq. 11 and 12).

$$ef = \frac{\sum r * \sum s}{n} \tag{11}$$

$$Kappa = \frac{\sum a - \sum ef}{n - \sum ef} \tag{12}$$

where r is the sum of the class-specific row values in the cross-tabulations, s is the sum of the class-specific column values, n is the total number of cases, ef is the expected frequency of each class, and a is the number of congruous cases.

The accuracies of the regression models in studies **II** and **III** were assessed in terms of degree of determination (R^2, Eq. 13), root mean square error (RMSE%, Eq. 14), and mean difference (MD%, Eq. 15). The R^2 value represents the proportion of variance in the dependent variable explained by the independent variables in the model. The RMSE% value describes the overall relative difference between the observed vs predicted values, i.e., the greater the percentage value, the greater the prediction error. The MD% value is also known as Bias and describes whether the expected value of the estimator is equal to the population parameter, which in our case indicates that if MD% is positive, then the model has a tendency for overestimation.

$$R^2 = 1 - \frac{\sum (y_i - \hat{y}_i)^2}{\sum (y_i - \bar{y})^2} \tag{13}$$

$$RMSE\% = \sqrt{\sum_{i=1}^{n} \frac{(y_i - \hat{y}_i)^2}{n}} \times \frac{100}{\bar{y}} \tag{14}$$

$$MD\% = \sum_{i=1}^{n} \frac{(\hat{y}_i - y_i)}{n} \times \frac{100}{\bar{y}} \tag{15}$$

where n is the number of observations, y_i is the observed value for observation i, $\hat{y}_i$ is the predicted value for observation i, and $\bar{y}$ is the mean of the observed values.

In study **II** the observed and predicted LFWD values (MN/m^2) were classified into trafficability categories according to the LFWD value thresholds in Table 4. These classification outcomes were further compared to obtain a percentage of agreement i.e. how accurately the categories of predicted LFWD values are similar to the categories of observed LFWD values. Also cross-tabulations were used to see how the categories classified from predicted LFWD values compared with the categories classified from the observed LFWD values.

Table 4. Thresholds for the LFWD values (MN/m^2) used in four different trafficability categories.

Category	All-year	Summer	Dry Summer	Winter
MN/m^2	>60	>50-60	30-50	<30

3 RESULTS

3.1 Comparison of gamma-ray datasets (study III)

The coefficients of the regression models are presented in Table 5. The correlation between the air gamma and ground gamma values was relatively low (Table 6). A separate model was constructed for each gamma component: potassium and thorium both exhibited moderate R^2 and correlation values, although the RMSE% value was quite high for both components (Table 5). The uranium component offered the weakest results across all statistics. Potassium got the best result with a normal linear regression ($R^2 = 0.294$), whereas uranium ($R^2 = 0.184$) and thorium ($R^2 = 0.263$) had better results with polynomial regression. The statistics for the uranium and thorium models showed minimal deterioration compared to the values in Table 6, even when simple linear regression was used. The uranium model yielded an R^2 value of 0.148 and an RMSE% of 0.561 while the thorium model yielded an R^2 value of 0.241 and an RMSE% of 0.487. In total, the polynomial models resulted in a relatively small improvement compared to simple linear regression. In all cases, the MD% value was small for all the models, so the risk of severe overestimation or underestimation was low. The fit of the regression lines of each model is shown in Figure 4.

Table 5. Polynomial regression to predict ground gamma-ray values using air gamma values. The predictions were made for each component, e.g., airborne potassium values were used to predict ground potassium values. Estimates and significance (p-value) of the different levels of predictors are shown.

Model information				
Potassium				
Coefficients	Estimate	Std. Error	t-value	p-value
Air K	0.844	0.034	24.570	2.00E-16
Uranium				
Coefficients	Estimate	Std. Error	t-value	p-value
Air U	2.291	0.374	6.131	8.19E-09
Air U^2	-2.095	0.529	-3.963	1.17E-04
Air U^3	0.653	0.180	3.628	3.98E-04
Thorium				
Coefficients	Estimate	Std. Error	t-value	p-value
Air Th	1.848	0.183	10.087	2.00E-16
Air Th^2	-0.122	0.041	-2.995	3.24E-03

Table 6. Statistics for polynomial regression predictions of each component. Pearson correlation was calculated from the normalized gamma values.

Statistics	Potassium	Uranium	Thorium
Pearson	0.543	0.384	0.491
R^2	0.294	0.184	0.263
RMSE	0.466	0.514	2.255
RMSE-%	0.515	0.548	0.481
MD%	5.50E-04	-8.57E-04	6.26E-03

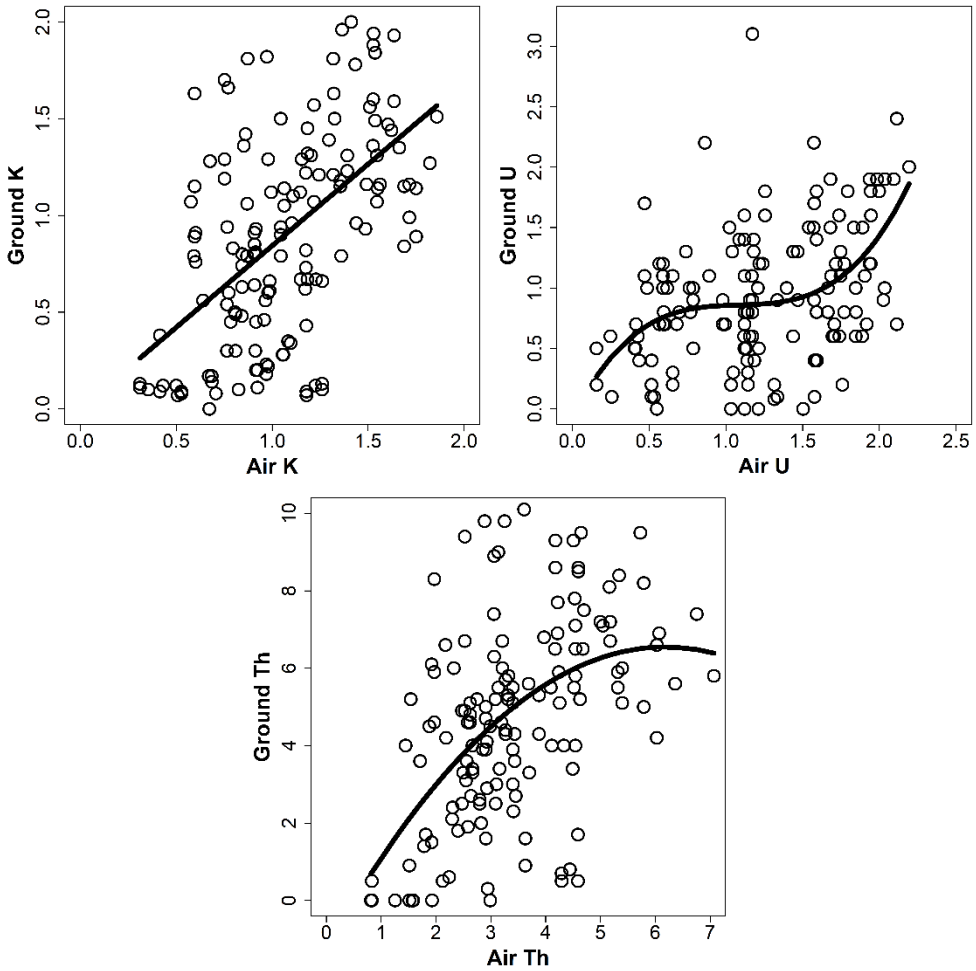

Figure 4. Ground gamma-rays vs air gamma-rays for each gamma component. The line indicates the regression line.

3.2 Prediction of bearing capacity (study II)

The correlations between light falling weight deflectometer values (LFWD)(MN/m^2), road properties, soil type and depth-to-water index are presented in Table 7. The significance of variables seems to be divided. Soil types peat and fine till (FT) and road properties useable road width (URW) and roadway width (RW) seem to have significant correlations with LFWD values. Sandy till has significant negative correlations (significant at the 0.01 *p*-level) with all the other soil types (peat (-0.51), sand (-0.44), fine till (-0.37)) which can partially be explained by the fact that it is the dominant dummy variable in our data and therefore an inverse dummy for the other soil types. The fine till variable has a significant correlation with LFWD values and both roadway width and useable road width. This matter is further considered in the discussion section.

The boxplots in Fig. 5 show the relations of the most important variables in the dataset of study **II**. The top left boxplot shows that there is a mixed trend with LFWD values and soil types with fine till having the highest LFWD values and sandy till and sand having slightly higher median LFWD values than peat. The top right boxplot shows that there is also an obvious trend between LFWD values and useable road surface width, where wider roads also acquire higher LFWD values, manifesting as significant correlation of 0.58 (Table 7). The lower left boxplot shows a correlation between low Ditch index values and the coarse soil type (sand), which means that in areas where soil type is sand, there are usually no or very shallow ditches. As illustrated in Fig. 5, there is considerable variation in the Ditch index for peat and sandy till. This variability can be attributed to the presence of road sections within these soil types that descend into the terrain. Consequently, the ditch depth is recorded as 200 centimeters, as detailed in the Materials and Methods section. The bottom right boxplot indicates a correlation between DTW values and the various soil types. However, it should be noted that DTW exhibits significant correlations with all soil types, with the exception of sandy till (Table 7).

Table 7. Topside of the table shows Pearson correlation coefficients between LFWD values, soil types, road properties, and Depth-to-water values. LFWD = Light falling weight deflectometer values, URW = useable road width, RW = roadway width, DTW = Depth-to-water index values, DI = Ditch index, Peat = peatland, ST = Sandy till, FT = Fine-grained till, Sand. Bottom side of the table shows the significance values of the correlations (p-values).

	LFWD	URW	RW	DTW	DI	Peat	ST	FT	Sand
LFWD		0.58	0.52	0.02	0.07	-0.25	-0.06	0.28	0.11
URW	0.00		0.90	0.15	0.13	-0.24	-0.11	0.38	0.07
RW	0.00	0.00		0.15	0.14	-0.32	-0.06	0.45	0.04
DTW	0.81	0.12	0.12		-0.21	-0.22	0.07	-0.21	0.33
DI	0.45	0.18	0.14	0.03		0.23	0.05	0.14	-0.45
Peat	0.01	0.01	0.00	0.02	0.01		-0.51	-0.2	-0.24
ST	0.54	0.25	0.53	0.43	0.58	0.00		-0.37	-0.44
FT	0.00	0.00	0.00	0.03	0.15	0.04	0.00		-0.17
Sand	0.24	0.47	0.71	0.00	0.00	0.01	0.00	0.07	

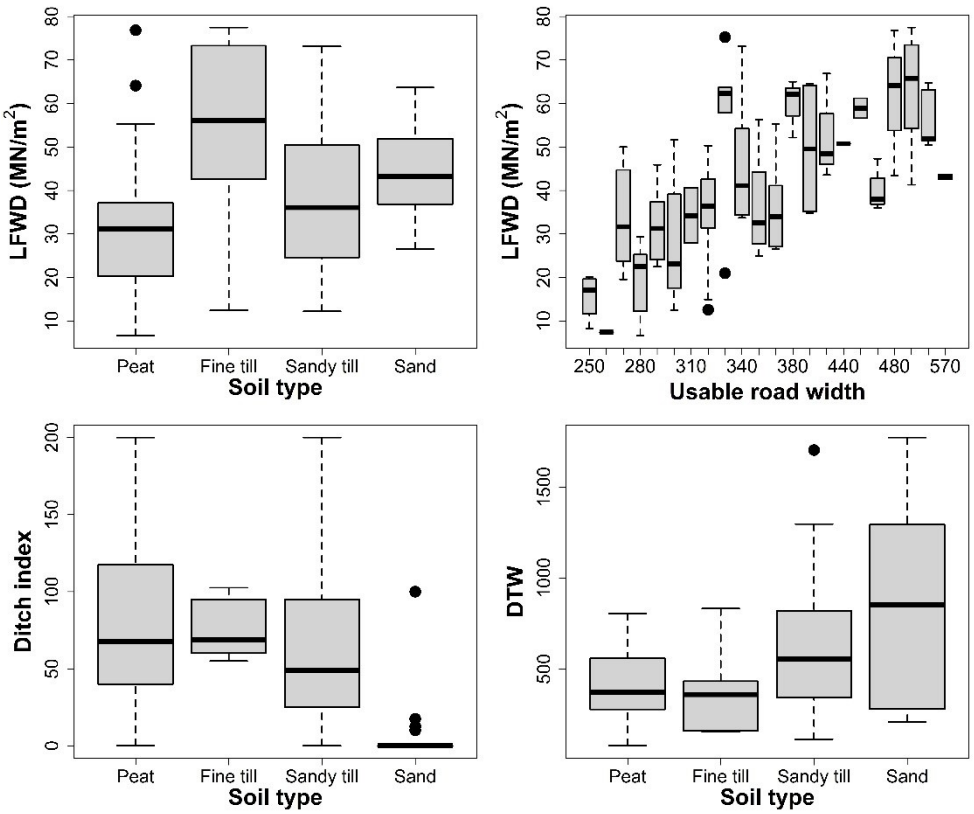

Figure 5. Boxplots for LFWD values and soil types (top left), LFWD values and useable road width (in centimeters) (top right), Ditch index (in centimeters) and soil types (bottom left), DTW index and soil types (bottom right). The ends of the box are the upper and lower quartiles, the median is marked by a horizontal line inside the box, and the whiskers extend to the highest and lowest observations. Figure created with R statistical computing environment (R Core Team 2020).

The plots on Fig. 6. present the gamma-ray components (K, U, Th) plotted against the LFWD values. The Pearson correlation coefficients are also presented on the plots which show that there is very little to no correlation between any of the gamma-ray components and LFWD values, with the highest being potassium (K) (0.11). The same observation can be seen from the plots themselves and the regression lines added to the plots which do not fit to the observations very well.

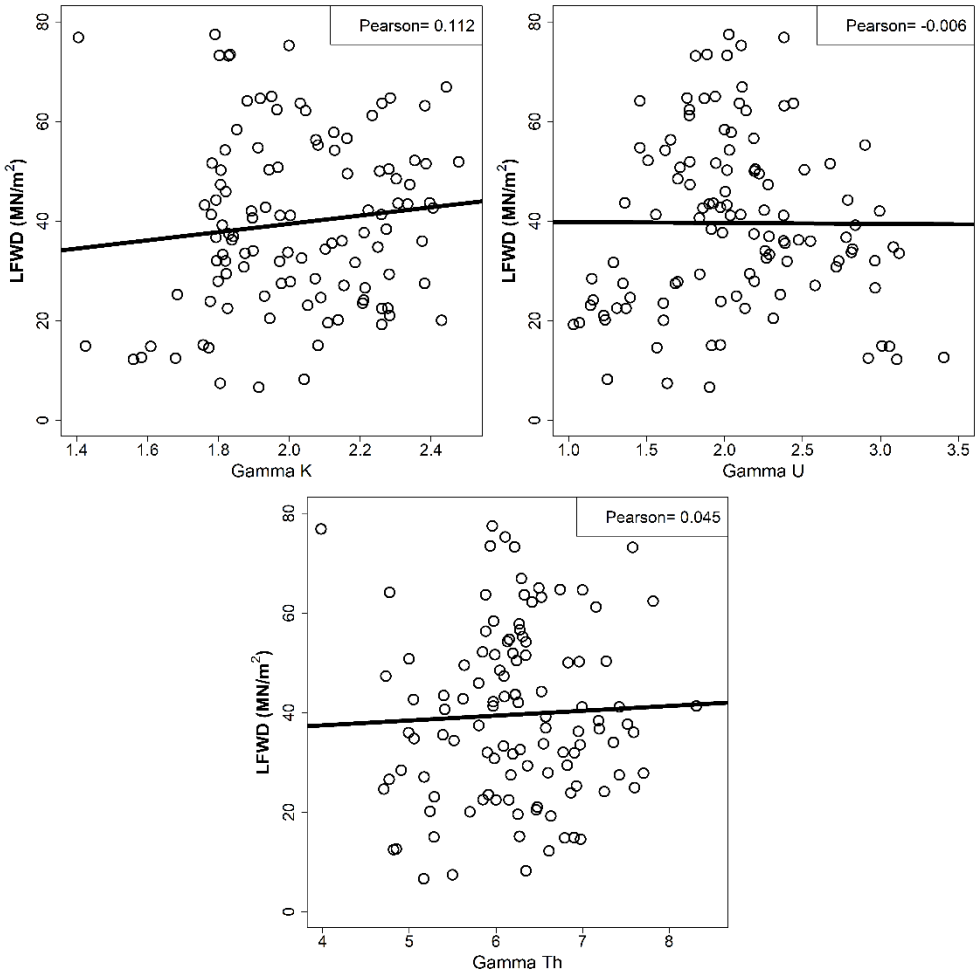

Figure 6. Plots of gamma values and LFWD values. Pearson coefficient in the top left corner of each plot reports the correlation between LFWD values and a single gamma component. The line on the plots represents the regression line when LFWD is predicted using each gamma component.

3.2.1 LME models for bearing capacity

Three linear mixed effects models were constructed using the significant road variables, soil type information and gamma-ray values. The soil types were transformed to soil coefficients as described in material and methods section. The road ID was used as the grouping variable in all models, so that the total number of groups (number of roads) was 25. The information given by all LME models is shown in Table 8. Stepwise selection for the first model (LME-1) resulted in useable road width emerging as the most significant variable at the 0.05 p-level. For LME-1 other variables did not reach the desired level of significance (p-value) but it was decided to include other variables to the model even though they would not reach significant

p-level. The used variables and their transformations can be seen from Table 8. Second model (LME-2) stepwise selection resulted, useable road width being significant at the 0.05 p-level and from gamma-ray values relative K being most significant still reaching only p-level of 0.24. The relative K value was calculated from the gamma-ray data by dividing the K component value with the sum of all components (K, U, Th). The third model (LME-3) was similar to LME-1 but it did not use useable road width (URW) as a variable since it performed too well, dropping the other variables from the model. Thus, the third model (LME-3) was constructed to see how significant effect the URW variable has in the resulting statistics. The variance inflation test for all models gave low values, the highest being 1.83 for the LME-3 for the variable roadway, and consequently the risk of multicollinearity in our models is low.

After LOOCV the LME-1 model acquired an R^2 of 0.315, LME-2 acquired R^2 of 0.335 and LME-3 acquired R^2 of 0.243 respectively. The LME-1 gained RMSE% of 35.7% before LOOCV and 36.0% after LOOCV, with a corresponding MD% value of -0.1% in both cases (Table 8), while the model with gamma-ray value (LME-2) had an RMSE% of 35.6% before LOOCV and 35.9% after LOOCV, with respective MD% values of -1.2% before and after LOOCV. Inclusion of the gamma-ray value (relative K) did not significantly improve the resulting statistics. LME-3 gained an RMSE% of 38.0% before LOOCV and 38.2% after LOOCV which is slightly worse than with models LME-1 and LME-2.

Table 8. Information obtained from the linear mixed effects models when fitted with all the data. The first section of the table includes estimates for all the variables used, with the standard errors given in parentheses. The second section includes p-values for all the variables used in both models, and the third section includes R^2, RMSE% and MD% statistics with no LOOCV and with LOOCV of both LME models.

	LME-1	**LME-2**	**LME-3**
Intercept	-	18.763 (12.972)	-
URW	10.617 (0.762)	9.176 (2.426)	-
RW	-	-	14.104 (1.044)
DI	1.712 (1.844)	-	-
(Soil * DTW)	0.040 (0.071)	-	0.049 (0.073)
K relative	-	-58.920 (49.791)	-
P(Intercept)	-	0.151	-
P(URW)	0.000	0.000	-
P(RW)	-	-	0.000
P(DI)	0.806	-	-
P(Soil * DTW)	0.040	-	0.038
K relative	-	0.240	-
Before LOOCV			
R^2	0.326	0.350	0.255
RMSE%	0.357	0.356	0.380
MD%	0.001	-0.012	0.014
After LOOCV			
R^2	0.315	0.335	0243
RMSE%	0.360	0.359	0.382
MD%	-0.001	-0.012	0.013

In the scatter plot of observed vs. predicted values after LOOCV (Fig. 7) a clear trend can be seen between observed and predicted values, but the relation does not seem to be completely linear. From Fig. 7 we can see that almost all low observed LFWD values (< 30 MN/m^2) are fitted to 30-35 MN/m^2 value range by the model. The residuals of the LME-1 do seem to have some variation, but it was not deemed to be significant in terms of functionality of the model. In the residuals we can spot the same trend as in the observed vs predicted plot, which is that the low observed values are predicted to much higher value range which is manifested as a high number of positive residuals among the low predicted LFWD values (x-axis). The scatter plots and residual plots of LME-2 and LME-3 were not significantly different and were therefore not added as a figure.

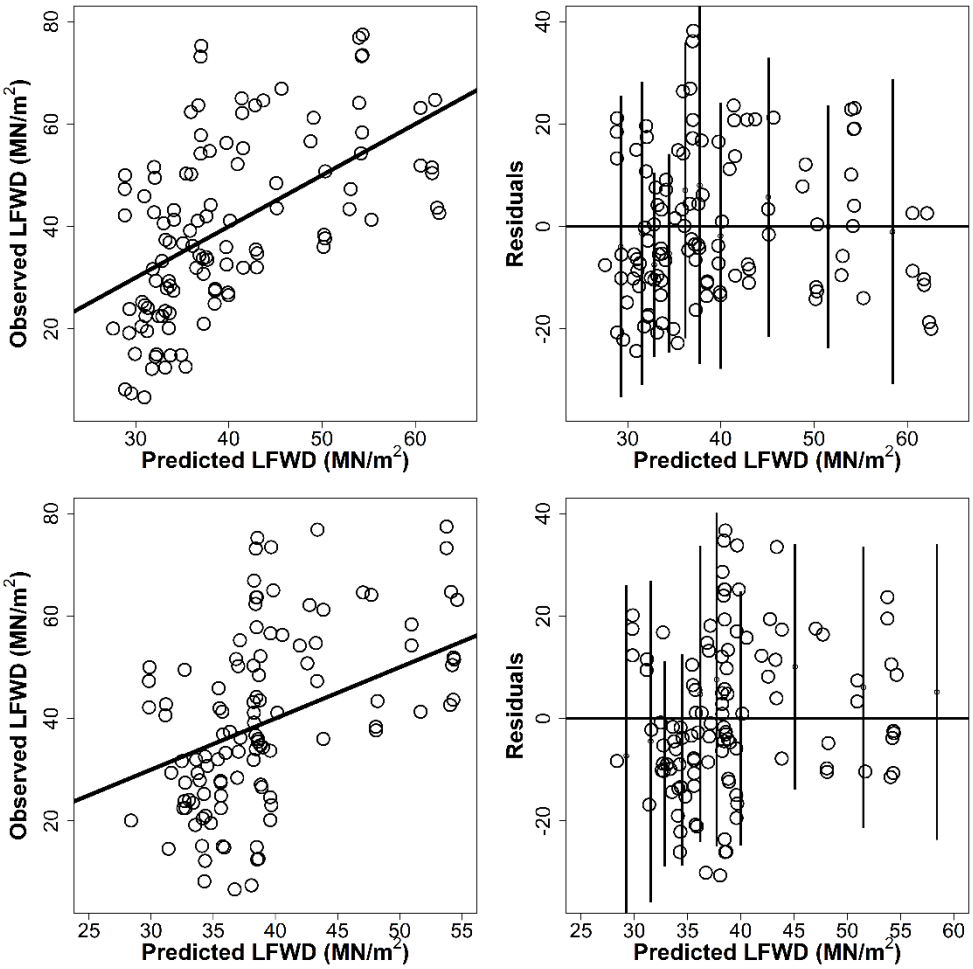

Figure 7. Upper figures show the plots from LME-1 and lower figures show the plots from LME-3. Left figure shows the plot of observed vs predicted LFWD values and the line which represents if these values had perfect linear relation. Right side figure shows the residuals of the model after LOOCV.

The observed and predicted LFWD values (MN/m^2) were classified into trafficability categories according to the LFWD value thresholds in Table 4. These classification outcomes were further compared to obtain a percentage of agreement (Table 9), i.e. how accurately the categories of predicted LFWD values are similar to the categories of the observed LFWD values.

Cross-tabulation of the predicted and observed trafficability classifications was used to see how the categories classified from predicted LFWD values fell into the categories classified from the observed LFWD values. The categories used in study **II** indicate the usability and trafficability of the road segments as was described in the discussion. The overall LFWD classification results are shown as percentage of agreement in Table 9. The classification results were calculated by subtracting the predicted category from the observed category (ordinal scale of trafficability categories). For instance, if the observed category was Summer (category 3) and the predicted category was also Summer (category 3), the prediction error value (Prer.) would be zero (0). Conversely, if the observed category was All-year (category 4) but the predicted category was Dry summer (category 2), the prediction error value (Prer.) would be negative two (-2). The classification results were consistent across all models, both before and after LOOCV, with a percentage of agreement ranging from 36.9% to 38.7%. The differences between classification results between the models were only marginal. Noticeable is that all of the models give high portion of one class over estimations (32.4%-37.8%). These misclassifications are the result of the over estimations of LFWD values which we observed in Fig. 7. where low observed LFWD values (< 30 MN/m^2) are all fitted by the models to the value range of 30-35 MN/m^2 in the predictions.

Table 9. Table shows the results of classifications obtained before and after LOOCV with different trafficability category thresholds. In the Prediction error (Prer.) column, a value of 0 indicates correctly classified observations with zero prediction error. The corresponding row displays the percentage of correctly classified observations (from the n=111 data) for each LME model. If the value in the 'Prer.' column is positive 1, it means that the classification overestimates the trafficability category by one category.

Model	Before LOOCV			After LOOCV		
Prer.	LME-1	LME-2	LME-3	LME-1	LME-2	LME-3
-2	0.090	0.090	0.117	0.090	0.090	0.117
-1	0.144	0.162	0.162	0.162	0.189	0.162
0	0.378	0.369	0.378	0.387	0.378	0.378
1	0.369	0.378	0.342	0.342	0.324	0.342
2	0.018	-	-	0.018	0.018	-

3.3 Prediction of soil and peat depths (study III)

The Spearman correlations between gamma-ray values and soil depths are presented in the captions of Fig. 8 (mineral soil) and Fig. 9 (peat soil). A negative trend was observed in both ground gamma and air gamma datasets concerning mineral soil depth and peat depth, indicating that gamma- radiation intensity in mineral soils decreases as the thickness of the soil layer overlaying bedrock or large boulders increases. Similarly for peat soils, gamma-radiation intensity decreased when the thickness of the peat layer covering the bedrock or subsoil increased. The air gamma components: potassium and uranium (Fig. 8), offered better Spearman correlations (K = -0.480; U = -0.474) with soil depth than ground gamma (K = -0.421; U = -0.238). In contrast, with regard to peat depths, ground gamma provided significantly better correlations across all components (K, U, Th) when compared to air gamma (Fig. 9).

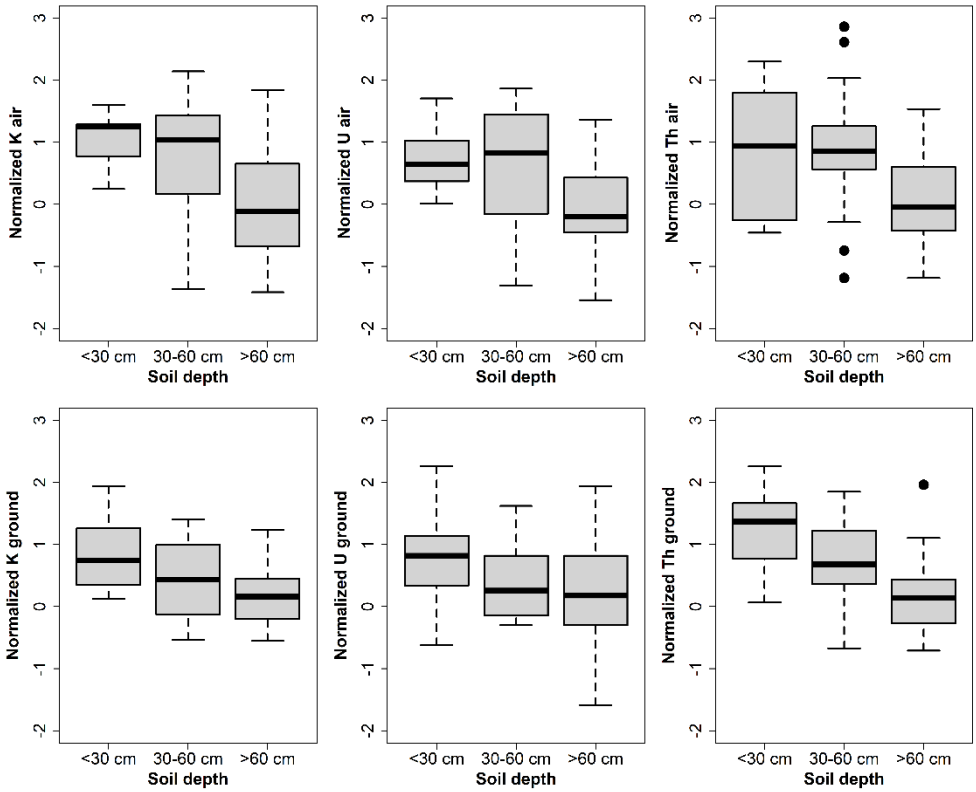

Figure 8. Boxplots of soil depth classes and normalized airborne gamma (upper row) and normalized ground gamma datasets (lower row) for mineral soils (n=85). The ends of the box are the upper and lower quartiles, the median is marked by a horizontal line inside the box, and the whiskers extend to the highest and lowest observations. Spearman correlations: K air = -0.480; U air = -0.474; Th air = -0.359; K ground = -0.421; U ground = -0.238; Th ground = -0.556

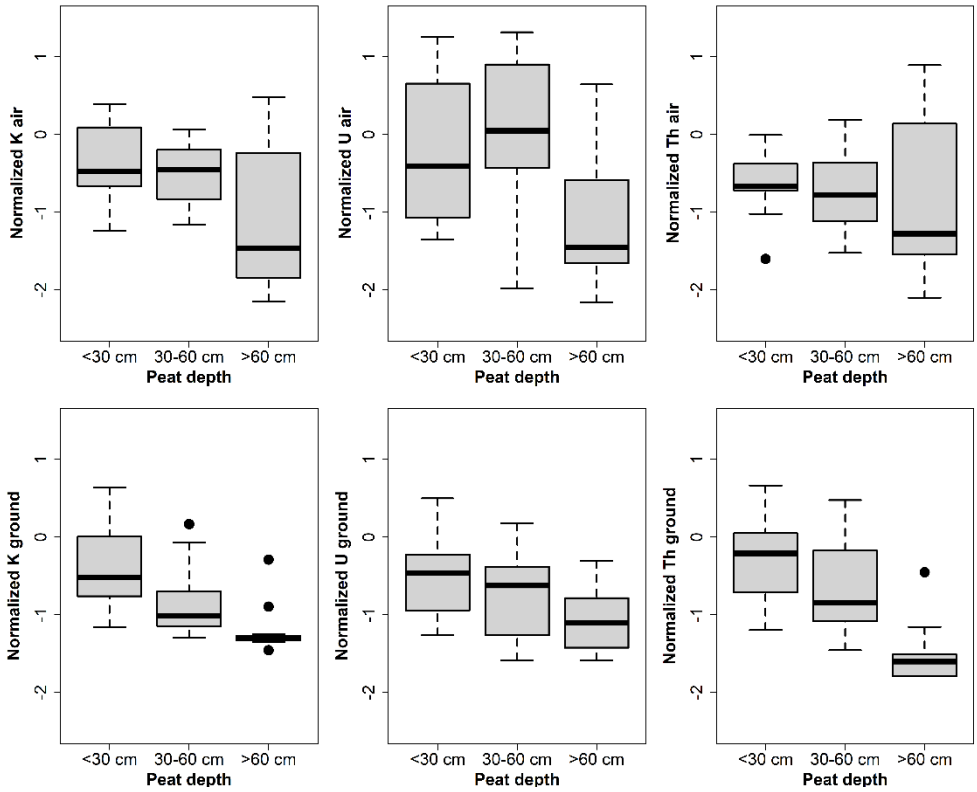

Figure 9. Boxplots of peat depth classes and normalized airborne gamma (upper row) and normalized ground gamma datasets (lower row) for peat soils (n=60). The ends of the box are the upper and lower quartiles, the median is marked by a horizontal line inside the box, and the whiskers extend to the highest and lowest observations. Spearman correlations: K air = -0.368; U air = -0.386; Th air = -0.243; K ground = -0.779; U ground = -0.409; Th ground = -0.762.

An ANOVA test was conducted for each gamma component to determine whether the mean values of each gamma component varied significantly (p-level <0.05) between soil depths. Our null hypothesis assumed that there was no significant difference in gamma values between the soil/peat depths. The ANOVA tests yielded significant results in every case, except between peat depth and the air gamma component thorium (correlation = -0.243). Therefore, we reject our null hypothesis and note that there was significant variation in gamma-ray values between the soil/peat depth levels (aside from air gamma thorium).

The prediction of soil depth was conducted separately for the mineral soil plots and peat soil plots. Ground gamma offered slightly better overall classification accuracies (64.7% mineral soil; 70.0% peat soil) when compared to air gamma (63.5% mineral soil; 61.7% peat soil). Soil depth predictions for the mineral and peat soils are shown in Fig. 10 and Fig. 11, respectively The plots in Fig. 10 show that the < 30 cm and 30–60 cm depth classes on mineral soils were interspersed, although the > 60 cm class was clearly separated, especially when predicted with ground gamma. For mineral soil depth predictions, air gamma offered

almost as good prediction result (63.5%) when compared to prediction result of ground gamma (64.7%) (Table 10). For peat soils, ground gamma provided a prediction result that was 8% better than the one provided by air gamma. Ground gamma showed a slightly better separation for the > 60 cm class on peat soil (depth 3, Fig. 11).

The functionality of all of the models was primarily influenced by the first discriminant function (LDA1). As the separation of classes occurred based on the LDA function on the x-axis (LDA1), there was minimal separation along the y-axis (LDA2) when visualized in the plots (Fig. 10 and 11).

Table 10. Classification statistics of the soil and peat depth models for air gamma and ground gamma datasets. The number of plots in each case is presented at the top of each section column. The 'count' rows represent the count of correctly predicted plots. The % rows represent the percentage of agreement (count/n). Kappa values are also presented for each case.

Soil depth	Mineral soil (n=85)		Peat soil (n=60)	
	Ground gamma	Air gamma	Ground gamma	Air gamma
Count	55	54	42	37
%	0.647	0.635	0.700	0.617
Kappa	0.458	0.414	0.599	0.497

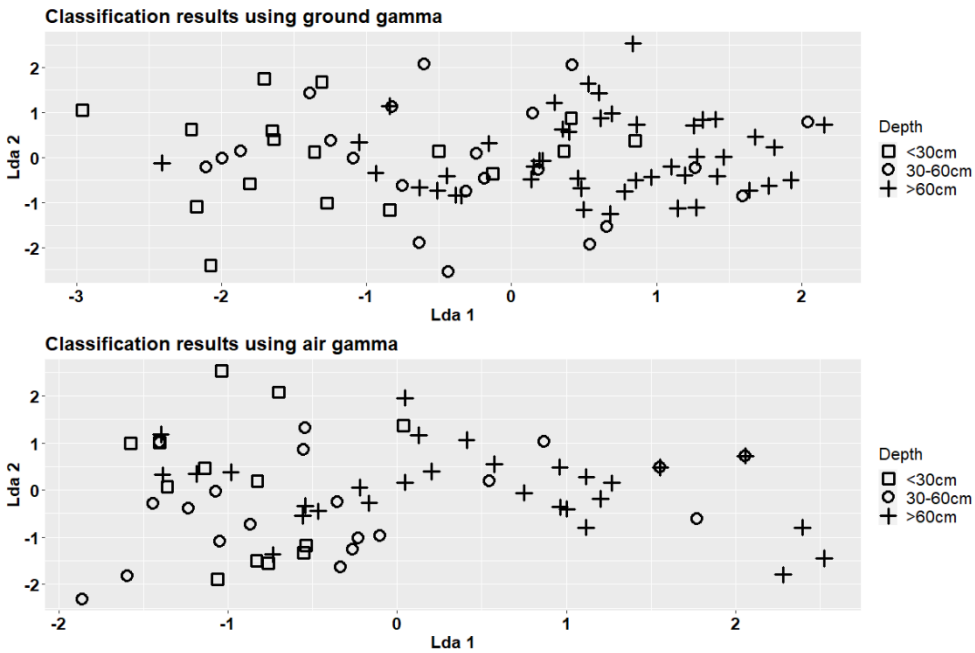

Figure 10. Distribution of soil depth classes when predicted with linear discriminant analysis (LDA) for mineral soils. The predictors used in the model were ground gamma components (upper graph) or air gamma components (lower graph).

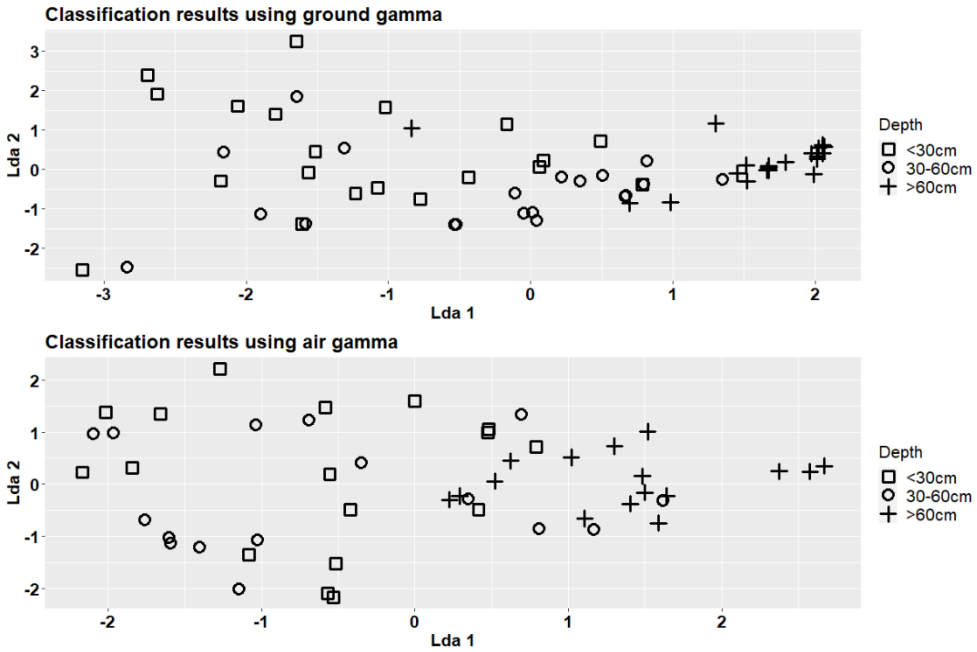

Figure 11. Distribution of soil depth classes when predicted with linear discriminant analysis (LDA) for peat soils. The predictors used in the model were ground gamma components (upper graph) or air gamma components (lower graph).

3.4 Prediction of topsoil stoniness (SI and SIC) study I and study III

The prediction of the stoniness of topsoil was carried out in studies **I** and **III** using the airborne gamma-ray data (studies **I** and **III**) and handheld gamma-ray spectrometer data (study **III**) as well as soil type information (studies **I** and **III**). In study **I** the stoniness was examined in terms of SI (0-10) and SIC with five levels (1-5) whereas in study **III** the stoniness was examined using only SIC with three levels (1-3). The study **I** utilized Ordinal regression as the main analysis method whereas in study **III** Linear discriminant analysis was used. The base assumptions required by the used analysis methods were met in both studies. In study **I** both peatlands and mineral soil plots (n=255) (Dataset 1) were included in the prediction of SI and SIC, but also separate dataset was selected which comprised only of mineral soil plots (Dataset 2). In study **III** only mineral soil plots were used in the modelling of SIC. In Study I the datasets were divided into training and validation samples whereas in study **III** LOOCV was used as the validation method.

The Spearman correlations between stoniness information, soil types and gamma values (both air gamma and ground gamma) showed significant relations among the variables in both studies **I** and **III**. The correlations of gamma-ray values and stoniness are presented in the caption of Fig. 12 for study **III** and in caption of Fig. 13 for study **I**. The correlation coefficients of the Dataset 1 (n=1221) in study **I** show strong correlation among air gamma values and SIC, with the highest observed coefficient being 0.634 (with component K). In study **III**, the correlation between SICs and air gamma values was moderate, with a highest

coefficient of 0.342 (with component K). However, it is important to note that study **III** utilized exclusively mineral soil plots in the data. Similarly, in study **I** the Dataset 2 also used only mineral soil plots and equivalent correlation with the highest coefficient of 0.368 (component K). The ground gamma values show higher correlation with SICs in study **III** with the highest coefficient of 0.605. In both studies **I** and **III** air gamma component uranium (U) gives the lowest correlation with SIC.

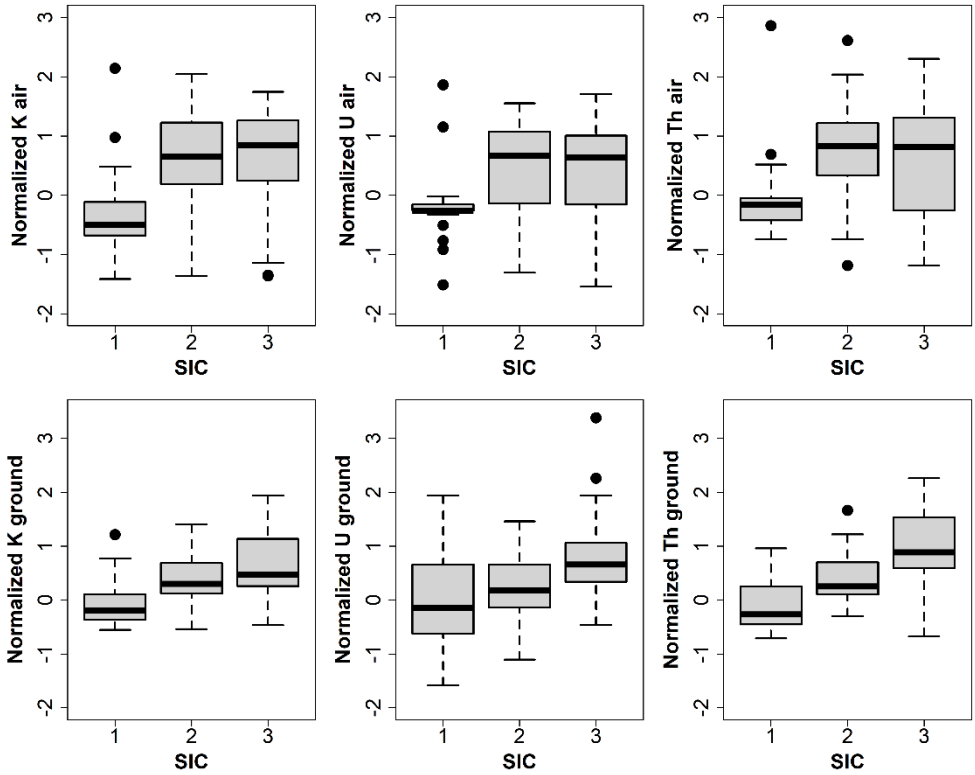

Figure 12. Boxplots of stoniness index classes (SIC) and normalized airborne gamma (upper row) and normalized ground gamma (lower row) datasets for mineral soils (n=85). The ends of the boxplots are the upper and lower quartiles, the median is marked by a horizontal line inside the box, and the whiskers extend to the highest and lowest observations. Spearman correlations: K air = 0.342; U air = 0.259; Th = air 0.276; K ground = 0.452; U ground = 0.395; Th ground = 0.607.

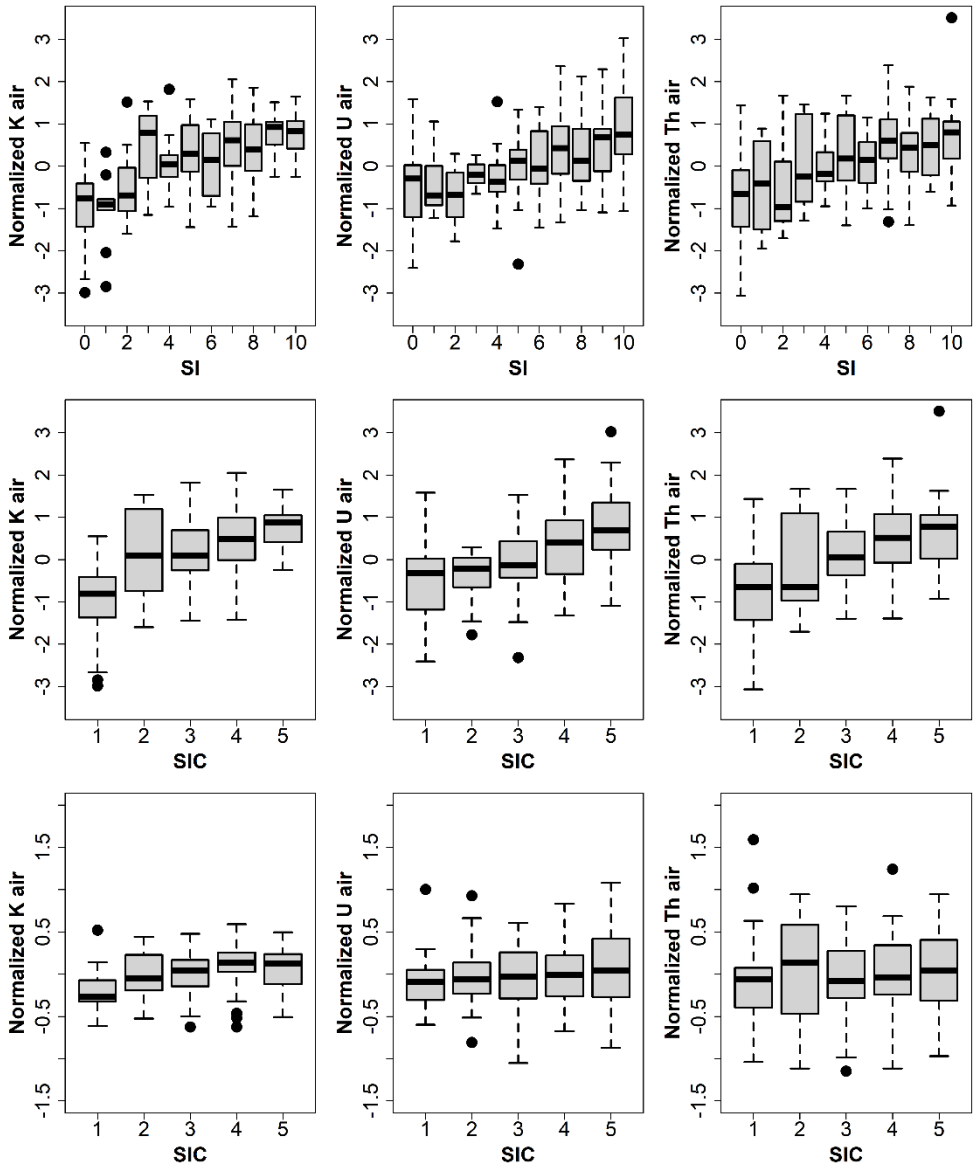

Figure 13. Boxplots for stoniness and their normalized air gamma values for whole dataset (SI top row, SIC second row) and for SIC of mineral soil dataset (bottom row). The ends of the box are the upper and lower quartiles, the median is marked by a horizontal line inside the box and the whiskers extend to the highest and lowest observations. Spearman correlations for whole data (Dataset 1) (rows 1 and 2): SI K = 0.621; SI U = 0.457; SI Th = 0.503; SIC K = 0.634; SIC U = 0.455; SIC Th = 0.508. Spearman correlations for mineral soil data (Dataset 2) (bottom row) SIC K = 0.368; SIC U = 0.157; SIC Th = 0.075.

3.4.1 Prediction of SI

In study **I** the ordinal regression managed to classify 36.47% of the SI cases correctly, with a kappa value of 0.199 and correctly with an acceptable two-class-off variation in 65.88% of the cases, with a kappa value of 0.587. The resulting crosstable (Table 11) showed that the correctly classified cases were divided between the extreme SI classes, in that only classes 0, 7, 8 and 9 had classifications in them, and the rest had none. When the SI model was tested with 500 randomly selected plots it managed to predict 29.00% of the cases correctly with a Kappa value of 0.000 and correctly with an acceptable two-class-off variation in 60.40% of the cases, with a Kappa value of 0.440. The resulting crosstable (Table 11) showed that the correctly classified cases were divided between classes 0, 7 and 8 while the rest of the SI classes had no correct classifications.

3.4.2 Prediction of SIC on mixed soils (Dataset 1) study I

In study **I,** using the whole data and the ordinal regression we managed to classify 52.16% of the SIC cases correctly in the modelling phase, with a Kappa value of 0.547, and correctly with an acceptable one-class-off variation in 78.82% of cases, with a kappa value of 0.719. The model informations are in Table 12. The resulting crosstable (Table 13) showed that the correctly classified cases were divided among all the SIC classes except for class 2, which had zero correct predictions. A total prediction error of three classes or over was observed in 7.45% of cases. In the testing phase the model achieved 49.00% prediction accuracy with Kappa of 0.478, and with acceptable variation the accuracy was 82.00% with Kappa of 0.766 which is an excellent result. The testing phase part of Table 13 shows that the classification again concentrates the sites into classes 1, 3 and 4. A total prediction error of three classes or over was only observed in 4.00% of cases.

Table 11. Crosstable of prediction of SI

		Modelling phase of SI				Testing phase of SI		
		0	7	8	9	0	7	8
SI	0	68	2	0	0	101	3	0
	1	9	0	0	0	15	2	0
	2	6	0	1	0	13	8	0
	3	4	5	1	0	12	11	0
	4	11	3	2	0	15	16	0
	5	5	9	4	0	22	31	0
	6	11	6	4	0	19	33	0
	7	7	13	9	2	17	41	0
	8	12	7	11	0	17	36	3
	9	4	5	10	1	13	23	0
	10	5	9	8	1	29	20	0

Table 12. Ordinal regression model predicting SIC classes based on dataset 1 using soil information and gamma values. Peat = Peatland, FT = Fine-grained till, Sand = sand, K = potassium gamma values, U = uranium gamma values. The intercepts in the model are class-pair specific and are used for calculating class-pair probabilities. The model uses a negative loglog link function.

Coefficients	value	std.error	t-value	p-value
Peat	-1.0557	0.232	-4.546	5.48E-06
FT	-2.7356	0.724	-3.780	1.57E-03
Sand	-0.4363	0.327	-1.335	1.82E-01
K	0.4672	0.113	4.128	3.67E-05
U	0.3997	0.109	3.658	2.54E-04
Intercepts				
1|2	-0.8041	0.128	-6.277	3.45E-10
2|3	-0.4604	0.121	-3.819	1.34E-04
3|4	0.4380	0.128	3.417	6.34E-04
4|5	1.6645	0.177	9.407	5.11E-21

Table 13. Correlation between observed (rows) and predicted SIC classes (columns) in the modelling and testing phases. Correct predictions are indicated with grey shading. The total numbers in the observed SIC classes in the test data (rows) were: SIC 1, n=121; SIC 2, n=44; SIC 3, n=136; SIC 4, n=114; SIC 5, n=85; and those in the testing phase results (columns) were: SIC 1, n=172; SIC 2, n=0; SIC 3, n=160; SIC 4, n=168; SIC 5, n=0.

		Modelling phase prediction of SIC					**Testing phase prediction of SIC**				
		1	2	3	4	5	1	2	3	4	5
SIC	1	70	0	8	1	0	110	0	9	2	0
	2	7	0	3	7	0	16	0	17	11	0
	3	12	0	22	20	1	21	0	64	51	0
	4	14	0	7	33	7	10	0	33	71	0
	5	4	0	7	24	8	8	0	29	48	0

The prediction of SIC was performed on mineral soils in both studies. The mineral soil dataset on study **I** consisted of 215 cases which had been manually picked to represent all the SIC classes evenly and it was divided into modelling and testing data in the ratio 0.7/0.3. The model information of study **I** can be seen in Table 14.

In study **I** during modelling phase (of Dataset 2) the ordinal regression managed to classify 32.24% of the cases correctly with a Kappa value of 0.181, and with acceptable one-class-off variation in 67.11% of cases with a Kappa value of 0.589 (Table 15). Each SIC class contained some correct classifications, but classes 1 and 4 possessed the highest numbers. In the testing phase the models achieved 28.57% prediction accuracy with a Kappa of 0.07 and with the acceptable variation 74.60% accuracy with Kappa of 0.671.

In study **III** the air gamma achieved prediction accuracy of 45.9% with a Kappa of 0.232 (Table 16) when using only gamma components as predictors. The result is slightly better

than in study **I** when not considering the acceptable one-off-variation, but of course in study **III** only three SIC classes are used. In study **III** the prediction accuracy increased noticeably with air gamma when soil type (mineral soil) was introduced to the model, now reaching prediction accuracy of 64.7% with Kappa of 0.499

Table 14. Ordinal regression model predicting the SIC classes of Dataset 2 using only gamma values for potassium (K), uranium (U) and thorium (Th). The model uses a cauchit link function.

Coefficients	value	std.error	t-value	p-value
K	3.2352	0.703	4.600	4.22E-06
U	0.0162	0.386	0.042	9.66E-01
Th	-0.8005	0.319	-2.507	1.22E-02
Intercepts				
1|2	-1.3347	0.201	-6.627	3.43E-11
2|3	-0.3205	0.123	-2.608	9.10E-03
3|4	0.5360	0.140	3.838	1.24E-04
4|5	1.7664	0.277	6.372	1.87E-10

Table 15. SIC classification results for both the modelling and testing phases with dataset 2

SIC	Modelling		Testing	
	Correct	Acceptable	Correct	Acceptable
Count	49	102	18	47
%	0.322	0.671	0.286	0.746
Kappa	0.181	0.589	0.066	0.671

Table 16. Classification statistics of the stoniness index class (SIC) models. Left shows the results with only gamma-ray values used as predictors, and the right shows the results with gamma-ray values and soil type used as predictors. The 'count' rows represent the count of correctly predicted plots. The % rows represent the percentage of agreement (count/n). Kappa values are also presented for each case. (n=number of plots)

SIC	Gamma only (n=85)		+ soil type (n=85)	
	Ground gamma	Air gamma	Ground gamma	Air gamma
Count	57	39	64	55
%	0.671	0.459	0.753	0.647
Kappa	0.579	0.232	0.673	0.499

The ground gamma performed noticeably better than air gamma. The ground gamma reached prediction accuracy of 67.1% with Kappa of 0.579 (Table 16) when using only the gamma components as predictors. When the soil type information was introduced along with ground gamma the prediction accuracy increased to 75.3% with Kappa of 0.647 (Table 16).

The SIC predictions of study **III** are shown in the upper and middle plots in Fig. 14 where it is evident that LDA had difficulty in separating the observations from the different classes. While ground gamma was able to separate the high-level and low-level SIC, there was considerable overlap between SICs of 1 and 2. Air gamma failed to clearly separate any of the SICs. When soil type was added to the models, the classification results improved for both ground gamma (by 8.2%) and air gamma datasets (by 18.8%). The addition of soil type to the model positively affected the separation of SIC classes (bottom plot in Fig. 14), especially the low stoniness class (SIC 1).

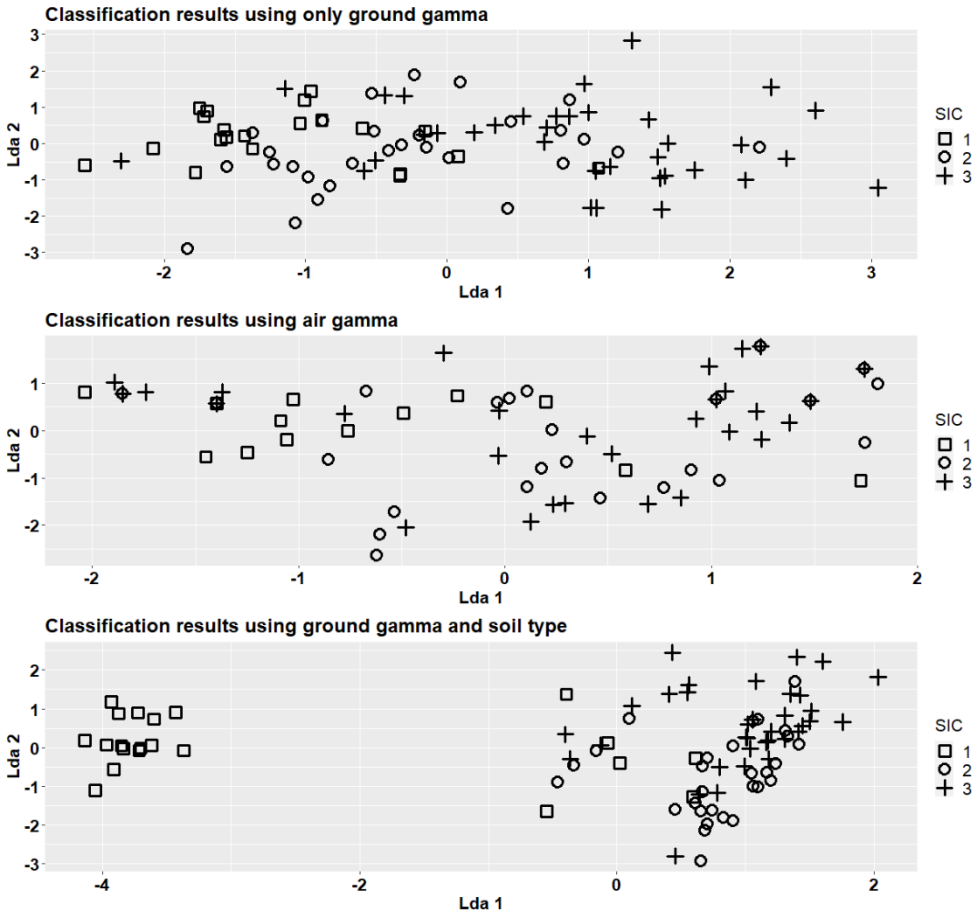

Figure 14. Distribution of stoniness index classes (SIC) when predicted using linear discriminant analysis (LDA) for mineral soils. The predictors used in the model are ground gamma components (upper graph), air gamma components (middle graph), or ground gamma components and soil type information (lower graph).

The functionality of all of the models in study **III** (both SIC and depth models) were primarily influenced by the first discriminant function (LDA1). As the separation of classes occurred based on the LDA function on the x-axis (LDA1), there was very little separation when the plots were viewed from the y-axis (LDA 2) (Fig. 10, 11, and 14). This observation was further supported by the proportion of trace of the functions (LDA 1 and LDA 2) acquired during the modeling process. In all SIC models, the proportion of trace was 90–99% for the first discriminant function (x-axis in Fig. 14) and 1–10% for the second discriminant function (y-axis in Fig. 14). In all soil depth models, approximately 90% and 10% of the separation was achieved by LDA1 and LDA2, respectively (LDA1 on the x-axis in Fig. 10 and 11, and LDA2 on the y-axis).

4 DISCUSSION

4.1 Comparison of airborne and ground gamma

The regression models for the gamma components yielded unsatisfactory results in study **III**. While potassium and thorium showed moderate R^2 and RMSE% values, uranium performed poorly (Table 6). Several factors likely contribute to these findings. Firstly, there is a significant time gap (30–40 years) between the airborne and ground gamma measurements, which allows for soil processes to alter the nuclide signature and the gamma spectra (e.g. Taylor et al. 2002; Herrmann et al. 2010). Additionally, anthropogenic activities such as soil preparation and peatland drainage can also affect the gamma fingerprint through the relocation and leaching of minerals, especially since the study sites were in active use of forestry. Studies by Takeuchi and Katase (1982) and Rizzo et al. (2022) suggest that short-term weather conditions, such as rainfall, can influence the intensity of gamma-rays. However, no weather data were recorded during the field measurements of study **III**, leaving uncertainty as to whether significant variations in short-term weather conditions near the time of measurement could have influenced the results. The most likely reason is the difference in resolution of the measurement methods. We know that gamma radiation is dependent on soil moisture and other soil properties (particle size, soil type etc.), which can vary greatly, even over small areas. Airborne gamma measurements provide low-resolution information (50 m × 50 m) whereas the handheld gamma offers almost point-type information that captures small-scale changes in soil properties. Minty (1997) emphasizes that airborne gamma surveys, while effective for large-scale surveys, has limitations due to its lower spatial resolution compared to ground-based methods. This lower resolution results from the wide field of view of airborne detectors, which average the gamma radiation over larger areas, potentially missing small-scale variations in soil properties.

In the study by Kock and Samuelsson (2011), a similar comparison of two gamma-ray datasets was conducted. While the airborne spectrometer scintillation units in their study were different from the units used in our dataset, the ground gamma spectrometers had a similar scintillation unit, although the device was manufactured by a different company. Moreover, Kock and Samuelsson (2011) studied continuous gamma-ray values whereas in study **III** a single measurement point type gamma-ray data was studied. They acquired high Pearson correlation coefficients between normalized airborne and normalized ground-based gamma-ray values: 0.98–0.96 for potassium (K), 0.68–0.94 for uranium (eU) and 0.97–0.92 for thorium (eTh), which are significantly better than the values reported in study **III** (Table 6). Their regression analysis also provided better results in terms of R^2 values for uranium

(R^2 = 0.82) and thorium (R^2 = 0.79) although their potassium R^2 value of 0.21 was weaker than observed in study **III** (Table 6). Kock et al. (2014) state that unknown radionuclide distributions, topography and geology as well can lead to uncertainties and problems when comparing ground gamma-ray measurements to airborne surveys which could be one explaining factor for the differing results. The observed differences in results are likely due to the geographical variability of the study areas. The study sites in Southern Sweden, as investigated by Kock and Samuelsson (2011), exhibit distinct mineralogical compositions and topographical features compared to study area location of study **III**. According to Kock and Samuelsson, the linear relationship between air and ground gamma measurements becomes apparent only in regions with significant variations in areal activity – a condition that our study area, characterized by homogeneity in parent mineralogy, does not meet. Additionally, the variation in topography between the sites may further contribute to the differences observed. Furthermore, Kock and Samuelsson's study benefited from a larger, more uniform study area and a substantially more extensive dataset, in contrast to our more limited and fragmented study site locations (relatively few measured plots scattered over large area).

4.2 The prediction of peat and soil depths

The soil depth classification results in study **III** were good for both the mineral and peat soils, with a clear trend of deeper mineral (Fig. 8) and peat soils (Fig. 9) as gamma values decreased. For mineral soils, there was practically no difference between using air gamma or ground gamma with both achieving prediction accuracies of around 64%. When the cross-tabulations of these classifications were evaluated, we noted that both gamma methods performed almost equally well at the >60 cm level. However, ground gamma performed better at the <30 cm and 30–60 cm levels which supports the superiority of ground gamma in this matter. For peat soil depths, ground gamma was almost 10% better than air gamma. Ground gamma effectively separated the peat depth observations at >60 cm and partially separated the observations at <30 cm and 30– 60 cm, while air gamma had difficulty separating observations at <30 cm and 30–60 cm levels (Fig. 9). Hyvönen et al. (2005) stated that, in general, the maximum thickness of a peat layer that gamma radiation can penetrate is 0.6 m which makes it a valuable method when predicting the depth of peat.

A substantial portion of Finland's original peat bog area was subjected to drainage for forestry purposes, during the 1960s and 1970s (Simola et al. 2012). In the year 2011, peatlands constituted approximately one-third of Finland's forestry area and one-fourth of the total growing stock volume (Ala-Ilomäki et al. 2011). However, this proportion has since changed due to the restoration of formerly drained bogs. Nonetheless, peatland areas still cover a substantial portion of the active forestry area. Lehtonen et.al. 2019 stated that the prediction of peat depth is important or future trafficability, as frost periods are becoming shorter due to global warming and so does the window for harvesting. In the future the decline in soil frost and wintertime bearing capacity will become increasingly evident. By the latter half of the 21st century, the majority of winters in southern and western Finland, will experience a virtual absence of soil frost in drained peatlands. A 20 centimeter thick layer of frozen soil or 40 centimeter thick layer of snow on the ground may already be sufficient for heavy forest harvesters (Lehtonen et al. 2019). This depth is optimal for gamma-ray surveys. Areas where peat depth exceeds 20 centimeters require deeper frost than areas with thinner peat depths. With precise peat depth data some clear-cutting operations located on peatland

stands scheduled to carry out in winter could be carried out during summer. This is due to the fact that clear-cutting allows for greater flexibility in selecting forwarding routes on-site in comparison to thinning (Lehtonen et al. 2019; Uusitalo et al. 2015).

4.3 Prediction of bearing capacity on forest road

The light falling weight deflectometer is commonly used as an alternative to the static plate load test (e.g. Sabouri et al. 2022). The FWD and LFWD are the most important devices used to evaluate the physical characteristics of road and soil surfaces (Kaakkurivaara et al. 2015). In Finland, forest roads are often constructed without compaction standards and with varying moisture and soil composition from materials found near the construction site (e.g. Grajewski, 2016). A few studies have suggested the potential value of applying gamma radiation surveys to estimate the proportion of clay in soil content (e.g. Díaz-Curiel et al. 2021). Therefore, in study **II**, the efficacy of these methods was assessed in predicting the bearing capacity and overall trafficability of unpaved roads.

Prediction of the overall trafficability of forest roads is extremely difficult. In study **II** the road width variable dominated, rendering other variables insignificant. Therefore, a decision to construct an additional model was made to see how much better prediction results the useable road width variable gives alone. Both useable road width (URW) and roadway width (RW) were powerful variables in every model which tells us that road width is a highly important factor when assessing bearing capacity which is also defended by the high correlation of road width variables and LFWD (Table 7). It is often safe to assume that wider roads are in better condition than more narrow roads since wide roads are often located in areas where there is more traffic from timber transportation and other vehicles. More narrow roads are built in areas where there are very little traffic, i.e. roads that lead to forest stands where there are fellings and the majority of traffic comes from timber transportation during certain seasons. There is potentially a need to develop separate models for high- and low-quality roads as differing road and environmental properties could influence the bearing capacity on different-sized roads.

It was surprising that the Ditch index was not a significant variable in any of the models and that there is very little correlation between the Ditch index and LFWD. The normal assumption is that low bearing capacity soil types (peat and fine till) should have high DI because ditches should usually be deeper on fine-grained soil types and peatlands, where conducting the water away from the vicinity of the road the frame is more crucial than in coarse soil types (sand and gravel). The Ditch index showed a significant correlation with certain soil types (peat and sand), which was expected since roads on coarse soils (sand) typically lack deep ditches, as water drains easily through the soil's pores.

The soil coefficients were significant variables when coupled with DTW but not when used alone. This defends one basic assumption regarding well-built forest roads which states that the surrounding soil type should not drastically affect the trafficability of the road if the road is built correctly, since if the building material available on site (i.e. the soil) is unsuitable (peat, fine till), the material for the construction of the supporting layers is generally brought from elsewhere. The surface layer of crushed rock is brought in from quarries. Of course, this assumption does not hold true for the majority of older roads, which have often been built without all the necessary structural layers. Since many old roads are not constructed with all the necessary layers and materials, it was expected that soil type could affect the bearing capacity. Some forest road networks consist of temporary roads constructed

from cheaper aggregates. For such roads, it would be reasonable to adopt different bearing capacity standards (Czerniak et al. 2021).

The R^2 statistics of models LME-1 and LME-2 show that the models performed moderately when predicting LFWD values. LME-3 had a noticeably (7%) lower R^2 value which was caused by the fact that LME-3 did not use URW as a predicting variable. The gamma-ray data unfortunately did not seem to be significant when predicting LFWD values. It can be observed from the plots and Pearson correlations of Fig. 6 that there is very little to no relation between gamma-ray values and LFWD. None of the gamma components prove to be significant in any of the models. Potassium achieved the best significance of all the gamma-ray components in LME-2 and offered only marginal improvement in the prediction results.

The overall prediction error (RMSE%) of all models was moderate, reaching values of around 36-38% which tells that there is considerable prediction error between observed values and predicted values. When assessing Fig. 7 we can see that models give overestimation in lower LFWD values and underestimation in higher LFWD values but all models still had low MD% (−1.2%−1.3%). We believe that the reason why our model failed to detect low LFWD values was because of the significance of the useable road width variable. Low-bearing capacity roads and some of the higher bearing capacity roads have similar widths, i.e. roads with a width of 350 centimeters include the majority of the low bearing capacity value roads but also a large part of the higher bearing capacity value roads. This causes the LFWD values to mix in the data which negates the lowest LFWD values from the predictions. As a solution, the modelling should be conducted where roads are divided to classes according to certain width thresholds and these classes could be used as the grouping variable if linear mixed effects models were to be used. Then it would be possible find the variables that have an effect on the LFWD values and are not tied to road width. In a study Varol et al. (2021) found that other methods (artificial neural networks; adaptive network based fuzzy inference system) than linear regression models perform noticeably better when predicting bearing capacity of forest roads. These methods could also be introduced to further studies.

In study **II** the classification of the trafficability categories performed poorly. This was largely the result of poor prediction accuracy of low LFWD values. The classifications achieved correct predictions only in 37.8% - 38.7% of cases. The crosstabulations of observed versus predicted classifications revealed that most predicted LFWD values were assigned to trafficability category 2 (dry summer), which has the widest LFWD range (30–50 MN/m²) and the highest case count. Consequently, other categories, such as winter, had only 1–2 correct classifications, and summer and all-year categories had very few correct classifications. This was caused by the overestimation of the models. The classification thresholds should be revisited at least on the account of Dry summer which seems to be too dominant compared to other categories and an additional category “Autumn” could be introduced to balance the categories. Autumn category roads would not be trafficable during spring thaw but still manage to maintain their bearing capacity and avoid rutting during the autumn, when there is high precipitation and fluctuating temperatures.

A similar study by Waga et al. (2021) has reported an overall classification accuracy of 77%, which is noticeably higher than that achieved in study **II** (36.9% – 38.7%). Waga et al. (2021) classified road condition with three categories (poor, satisfactory, good) using the Topographic Position Index together with LiDAR and DEM data, in order to determine the need for road rehabilitation. Their quality categories were based on visible parameters defined by experts (Korpilahti, 2008), whereas study **II** was focused on estimating a non-

visible parameter (LFWD) using road structure variables. In the approach used by Waga et al. (2021) the estimation of forest road quality and surface condition (surface wearing and flatness) was based on a total of 62 plots and was carried out subjectively, which leaves room for human estimation error. Study **II** used a slightly larger dataset of 111 plots together with LFWD measurements to determine trafficability classifications in terms of 4 categories. The method implemented by Waga et al. (2021) is prone to a risk of subjective autocorrelation since all the road parameters are visually evaluated, which can partially explain the better classification results.

In study **II** it was known that the prediction of bearing capacity without having information on the road's supporting layers and construction materials would be challenging and overall, it must be said that the models, did not produce satisfactory results. The static road and surrounding terrain properties used here were not enough to provide good predictions of the bearing capacity. In order to address this issue, more variables should be introduced into the model to test whether they result in a significant improvement relative to the LFWD predictions. Even though the soil type did seem to be significant in this work, soil type information should be included in future models as an alternative dummy variable. The problem is that accurate soil type information is not always available. The existing soil maps of Finland (Geological Survey of Finland, 2024) are often published at a scale of 1:20 000 or 1:50 000 and in many areas at a coarser scale of 1:100 000 or 1:200 000, and the principal soil types recognised are often sandy till or peat, which were not significant in this study.

One major defect with our model was the lack of road surface information, which is often the most significant variable when considering rutting and bearing capacity. Surface quality information could be derived from LiDAR data if these are dense enough (12 pulses m^2 (James et al. 2007; Waga et al. 2021)) as observed previously (Craven and Wing, 2014; Waga et al., 2015, 2016, 2021), and other road properties such as the centre line, road frame width, ditch depth and ditch quality could be extracted from ALS data if these are dense enough (Azizi et al. 2014; Craven and Wing, 2014; Ferraz et al. 2016; Hrůza et al. 2018; Waga et al. 2015, 2016, 2020, 2021; Karjalainen et al. 2024). For this purpose, the 5P data provided by the National Land Survey of Finland could have been used to some extent. Surface condition significantly affects bearing capacity, particularly during high precipitation, which increases moisture content in the road surface. Aleadelat et al. (2017) also demonstrated the use of smartphone sensors in evaluating gravel road conditions with promising results especially detecting potholes and surface deterioration. Kaakkurivaara et al. (2016, 2017) state that mixing ash into the crushed rock surface layer of a forest rod will form a tough shell that can significantly increase the bearing capacity. On soils with limited bearing capacity, such as wetlands, the use of geotextile mattresses has proven to be an effective solution. Research has demonstrated that, despite the recorded bearing capacity during testing being low, these pavement systems offer good performance for periodic forest management operations (Czerniak et al. 2021).

The bearing capacity of forest roads is influenced by moisture levels, which significantly impact the structural integrity of road surfaces, as highlighted by Elshaer et al. (2018). Similar findings were reported by Salour and Erlingsson (2013), who investigated pavement structural behavior during the spring thaw. Their use of a falling weight deflectometer demonstrated that the thawing process, which increases water content, in combination with traffic loads, can substantially affect pavement lifespan and alter the mechanical properties of the road. This warrants the development of bearing capacity models that account for both static and dynamic road and environmental factors.

4.4 Topsoil stoniness and gamma-ray data

When assessing the data of studies **I** and **III** (Tables 1 and 2), it is evident that SIC levels and gamma-ray values have a clear parallel correlation between gamma values and SIC levels, which can also be clearly seen in Fig. 12 and 13. This is also supported by the mostly high correlation coefficient between SICs and gamma components in the data of both studies, except for the mineral soil data from study **I**. The trend is not as clear in the SI figures, and the gamma values do not increase consistently with the SI classes (Fig. 13). The clearest correlation with SIC and gamma is achieved by the ground gamma values, which performed better than air gamma in predicting SIC. The difference in the correlations between the studies is due to the difference in composition of the datasets, where in study **I** peatlands were included in the main dataset and in study **III** only mineral soils were used.

In study **I** the overall results of the SI predictions were better than expected achieving accuracies of 36.47% - 65.88% but the ordinal regression had major difficulties in creating boundaries between most of the SI classes. Only some of the SI classes had correctly assigned values on them and on Table 1 we can see how only the gamma values of extreme SI classes are separated from the mid-section values. The good performance of the model in the low SI classes can be explained by the fact that a large number of the sample plots with low SI values were on peatlands, where the soil contains large amounts of water. An increased moisture content in the soil reduces the intensity of the gamma radiation and in peatlands, the average moisture content of peat is around 90% (Hyvönen et al. 2005). Peatlands are also known for having relatively small quantities of stones as compared to mineral soils. There was evident autocorrelation between peatlands, stoniness, and low gamma values which presumably caused the SI predictions to achieve as good overall results and high correlations (caption of Fig. 13). This was indicated by the increased VIF-score (4.04) for variable peat which causes some uncertainty towards the performance of the model but was not considered being a severe violation in this case. The model also performed moderately well among the high SI classes, in which high SI values were typically obtained in areas where bedrock or large boulders lay close to the ground surface. It is known that the intensity of gamma radiation is affected by the grain size of the mineral particles in a soil (Hyvönen et al. 2005), the larger the particle, the higher the emitted radiation – which explains the correlation between high gamma-ray values and SI findings in study **I**. When interpreting the class probabilities acquired from ordinal regression, most of the values were quite evenly distributed among several SI classes. The results indicate moderate performance at the extremes of the scale but poor overall accuracy of SI predictions.

In study **I** the results of SIC prediction based on whole dataset, which also included peatland plots, were good in both the modelling and testing phase, reaching 49% - 82% prediction accuracies and the prediction errors of three classes or over were only 7.45% at most. However, as can be seen from Table 13, the SIC had similar problem to SI, where there is classes (SIC 2) with zero correct predictions. Furthermore, the SIC 1 achieved high correct prediction percentage of ~90%, which is most likely result of the previously described autocorrelation (low stoniness, peat soil, and low gamma-ray values), where peatlands contain smaller quantities of stones compared to mineral soils and have low gamma-ray values due to high moisture content in the soil. Therefore, for study **III** the SIC predictions were carried only on mineral soils as was done also in study **I** with separate dataset (Dataset 2).

In study **III** we created two separate models for SIC, as the plots composed mainly of fine till were all assigned to the low-level stoniness class (SIC 1), which we thought would

cause an imbalance in the model. The results of study **III** indicated that the inclusion of soil type had a slight improving effect on the classification results, which was expected. The models that used air gamma data as the predicting variable obviously benefited more from the inclusion of soil type (percentage of agreement increased by 18%) compared to the models that used ground gamma data (percentage of agreement increased by 8%).

The SIC models in study **III** (using only gamma values) that used the ground gamma data achieved over 20% better classification accuracy than the models that used air gamma data. The air gamma data had difficulty separating SIC 2 from the other classes, resulting in a lower prediction accuracy. The difference in classification accuracy is due to the averaging nature of air gamma data, which misses the small-scale variations but which are detected by the handheld device (Minty, 1997). Compared to Studies **I** and **III** Melander et al. (2019) reported similar results, achieving 70% accuracy in their study of topsoil stoniness prediction (with three SIC) using excavator boom vibration data. This outcome enhances the reliability of the finding that topsoil stoniness can be predicted through different methods, particularly when employing classification techniques. However, both methods have limitations: the approach used by Melander et al. (2019) is applicable only during soil preparation, and the constraints of gamma spectrometry are extensively discussed earlier in this dissertation.

Heiskanen et al. (2020) conducted a study in which they predicted the stone volume of topsoil (0–30 cm) in Finland using airborne gamma-ray data (specifically the K component). They achieved relatively low prediction accuracy, with an R^2 of 17%. Their study area covered all of Finland so there is a major variation in parent mineralogy which may have affected their result compared to studies **I** and **III**. Additionally, the analytical methods differ where Heiskanen et al. (2020) predict the volumetric stoniness using general linear models rather than classification. In a study by Priori et al. (2014) they used similar gamma-ray data to predict soil stoniness, achieving a moderate R^2 of 41%. Their study was conducted in a topographical area where the mineral composition and parent material differ significantly from those in the study area of studies **I** and **III**. Additionally, their study area exhibited substantial variation in parent materials which most likely led to the differences in the results. Soil textures often show reliable correlation with soil gamma radiation and can be quite easily used to predict soil texture in areas characterized by homogeneous parent material. In regions where the lithology is heterogeneous, more advanced statistical processing is required for data aggregation in order to derive textural information. (Reinhardt and Herrmann 2018). Therefore, it is important to acknowledge that soil mapping using gamma-ray spectrometry strongly site-specific (Dierke and Werban 2013; Priori et al. 2014; Rawlins et al. 2007).

The volumetric proportion (%) of stoniness in soil would offer a better overall picture of the stone content, as demonstrated by Heiskanen et al. (2020). However, as seen in Studies **I** and **III** and in Melander et al. (2019), classification of stoniness provides more consistent and accurate prediction results (compared to prediction accuracy of Heiskanen et al. (2020) and Priori et al. (2014)) even if, the measurement methods differ. The bedrock in our study area showed little variation (consisting mainly of migmatite) which is crucial, as previous research has stated the radiation properties of soil are affected more by the parent material, rather than individual soil characteristics. In addition to gamma values, we could consider using information on above ground boulders to assist in the prediction of topsoil stoniness. As evidenced by Stendahl et al. (2009), a correlation was identified between surface boulder frequency and stone and boulder content. However, the strength of this correlation exhibited regional variations. Furthermore, the correlation between stoniness and soil information with different landforms and topographies should be considered. Digital terrain models (DTMs) would be useful in this regard, as they can be created using data obtained from various

sources, such as ALS and TLS, which are extensively employed in forest inventories (Hyyppä H. et al. 2005; Hyyppä J. et al. 2006; Hyyppä H. et al. 2006).

In a study by Kankare et al. (2019) they evaluated the information of the static trafficability map in relation to the rutting damage within logging tracks within thinning stands. They stated that the probability of rutting damage is found to be considerably influenced by a variety of factors, including local weather history, route planning and used machinery. An analysis of the available data indicates that the utilization of static trafficability maps can enable the allocation of harvesting stands for different seasons, thereby providing a framework for the strategic planning of wood procurement. Terrain trafficability maps are widely available and undergo continual improvement and refinements (Finnish Meteorological Institute 2023; Metsäkeskus 2023). However, trafficability maps have a somewhat coarse resolution and further research is necessary to comprehensively understand the impact of various variables on the risk of rutting damage. As study **III** concluded, a handheld gamma spectrometers could be used to observe small-scale changes of the soil more accurately. Of course, measurements with handheld gamma spectrometers are laborious for large scale usage but could be utilized on some smaller areas. Gamma spectrometers that can be attached to drones could provide valuable information on the small-scale changes in soil properties that have an impact on trafficability. Klvac et al. (2010) suggest based in their study that light falling weight deflectometer (LFWD) may be utilized to assess the bearing capacity and compaction of forest soils beneath the canopy as well as in transport lines. This data could be studied in conjunction with gamma-ray data. Although, study **II** found no correlation between LFWD values and gamma values, this has not been studied in the field of terrain trafficability.

Capturing within-site variations in site trafficability is necessary to avoid undesirable soil and root damage. Hoffman et al. (2022) stated that DTW maps are an effective tool in forest management when planning and executing operations in order to mitigate the traffic-induced soil impacts, by identifying sensitive areas that should be avoided during mechanized operations. Highest degree of rutting and soil compaction typically occurs in the top 30-centimeter soil layer, which normally contains most of the root mass (Wingate-Hill and Jakobsen, 1982). All of these effects on the soil structure can significantly reduce vegetation growth. Murphy et al. (2004) reported that compaction below a depth of 10 centimeters resulted in a reduction of up to 42% in tree growth, which corresponded to a 60% reduction in value over a projection of 28-year period. Pressure and rutting can be avoided by creating brush mats from harvesting residues especially for peak loads on the most vulnerable sections of stands (Labelle and Jaeger 2012).

5 CONCLUSIONS

Predicting the bearing capacity and trafficability of forest roads by means of static road parameters remains a challenge. Addressing the problem related to detecting weak spots on roads is imperative, as gamma-ray data did not provide any insight on that matter. Furthermore, the classification thresholds (Table 4) should be validated through testing and field measurements, as there is currently little information on how they are actually delimited/formed and whether they can be properly used in practice. Additionally, an alternative analysis method to LME should be considered as the results of this dissertation demonstrate that the relationship between road properties and LFWD values is not linear.

While road width variables appeared to be highly significant in detecting LFWD values, other significant variables need to be identified due to autocorrelation with road quality and road size. In particular, water content and the condition of the road surface and underlying layers are likely to enhance the accuracy of assessments regarding the bearing capacity of roads in general. The increasing availability of dense LiDAR data available in Finland could provide a useful tool for extracting data on these significant road properties without extensive and laborious field measurements and should thus lead to improvements in the planning and targeting of road maintenance.

The results of this dissertation provide novel insights into the application of gamma-ray spectrometry for assessing soil properties which affect the terrain trafficability. The study makes successful predictions regarding the stoniness of topsoil and offers encouraging results for predicting soil and peat depth. Whether these results are applicable on geologically diverse settings remains unclear or if a petrologic adjustment factor is needed. To achieve a more comprehensive assessment of the method's robustness across diverse environments, further studies are necessary. These studies should employ larger datasets and high-resolution gamma data on varying parent materials. The study-specific results also highlight the potential of ground gamma/high resolution gamma to noticeably improve the prediction of soil properties when compared to air gamma.

REFERENCES

Ågren, A. M., Lidberg, W., Strömgren, M., Ogilvie, J., Arp, P. A. (2014). Evaluating digital terrain indices for soil wetness mapping– A Swedish case study. Hydrology and Earth System Sciences, 18(9), 3623–3634. doi:10.5194/hess-18-3623-2014

Äijälä et al. 2014. Metsänhoidon suositukset. Metsätalouden kehittämiskeskus Tapion julkaisuja. Available: http://www.metsanhoitosuositukset.fi/suositukset/metsanhoidonsuositukset/ (In Finnish)

Ala-Ilomäki J., Högnäs T., Lamminen S., Sirén M. (2011). Equipping a conventional wheeled forwarder for peatland operations. International Journal of Forest Engineering 22(1): 7–13.

Ala-Ilomäki, J., Salmivaara, A., Launiainen, S., Lindeman, H., Kulju, S., Finér, L., et al. 2020. Assessing extraction trail trafficability using harvester CAN-bus data. Int. J. For. Eng. 31(2): 138–145. doi:10.1080/14942119.2020.1748958

Aleadelat, W., Wright, C., Ksaibati, K. (2017). Estimation of Gravel Roads Ride Quality through Android-based Smartphone. Transportation Research Record Journal of the Transportation Research Board. 2672. doi:10.1177/0361198118758693

Ashby, W.C., Vogel, W.G., Kolar, C.A., Philo, G.R. 1984. Productivity of stony soils on strip mines. In Erosion and productivity of soils containing rock fragments. Vol. 13. Edited by J.D. Nichols, P.L. Brown, W.J. Grant. doi:10.2136/sssaspecpub13.c4

Azizi, Z., Najafi, A., Sadeghian, S. (2014). Forest road detection using LiDAR data. Journal of Forestry Research, 25(4), 975–980. doi:10.1007/s11676-014-0544-0

Bygdén, G., Eliasson, L., Wästerlund, I. 2003. Rut depth, soil compaction and rolling resistance when using bogie tracks. J. Terramech. 40: 179– 190. doi:10.1016/j.jterra.2003.12.001.

Cambi, M., Certini, G., Neri, F., Marchi, E. 2015. The impact of heavy traffic on forest soils: a review. The impact of heavy traffic on forest soils: a review. For. Ecol. Manage. 338: 124–138. doi:10.1016/j.foreco.2014.11.022

Cook, S., Corner, R., Groves, P., Grealish, G. 1996. Use of airborne gamma radiometric data for soil mapping. Soil Res. 34:183–194. doi:10.1071/SR9960183.

Craven, M., Wing, M. G. (2014). Applying airborne LiDAR for forested road geomatics. Scandinavian Journal of Forest Research, 29(2), 174–182. doi:10.1080/02827581.2014.881546

Czerniak, A., Grajewski, S., Kurowska, E. (2021). Bearing Capacity Standards for Forest Roads Constructed Using Various Technologies from Mechanically and Chemically Stabilised Aggregate. Croatian journal of forest engineering. 42. doi:10.5552/crojfe.2021.996.

Díaz-Curiel, J., Miguel, M., Biosca, B., Arévalo-Lomas, L. (2021). Gamma ray log to estimate clay content in the layers of water boreholes. Journal of Applied Geophysics, 195. doi:10.1016/j.jappgeo.2021.104481

Dickson, B.L., Scott, K.M. 1997. Interpretation of aerial gamma-ray surveys adding the geochemical factors. J. Aust. Geol. Geophys. 17:187–200.

Dierke, C., Werban, U. 2013. Relationships between gamma-ray data and soil properties at an agricultural test site. Geoderma, 199: 90–98. doi:10.1016/j.geoderma.2012.10.017

Dong, D., Li, Z. (2021). Smartphone Sensing of Road Surface Condition and Defect Detection. *Sensors*, *21*(16), 5433. doi:10.3390/s21165433

Eliasson, L. 2005. Effects of forwarder tyre pressure on rut formation and soil compaction. Silva Fenn. Monogr. 39: 549–557. doi:10.14214/sf.366

Eriksson, C.-P., Holmgren, P. 1996. Estimating the stone and boulder content in forest soils — evaluating the potential of surface penetration methods. Catena, 28: 121–134. doi:10.1016/S0341-8162(96)00031-8.

Ferraz, A., Mallet, C., Chehata, N. (2016). Large-scale road detection in forested mountainous areas using airborne topo graphic lidar data. ISPRS Journal of Photogrammetry and Remote Sensing, 112, 23–36. doi:10.1016/j.isprsjprs.2015.12.002

Finnish Meteorological Institute. 2023. Harvester seasons. Finnish meteorological institute. [accessed 2023 March 1st]. https://harvestersea sons.com/

Geisler, E., Rittenhouse, C.D., Rissman, A.R. 2016. Logger perceptions of seasonal environmental challenges facing timber operations in the upper Midwest, USA. Soc. Nat. Resour. 29(5): 540–555. doi:10.1080/08941920.2015. 1107789.

Geological Survey of Finland (GSF). (2024). File service of open soil data– Maankamara. Retrieved June 6, 2021, from https://gtkdata.gtk.fi/Maankamara/index.html

Geological Survey of Finland. 2020. File service of open data. Available from https://hakku.gtk.fi/en [accessed 6 May 2020].

Georadis O. 2023. Georadis GT-40 multifunctional gamma ray spectrometer. [assessed 2023 Jan 6]. http://www.georadis.com/en/pro ducts/gt-40.html .

George K.P., Uddin W. (2000). Subgrade characterization for highway pavement design. Final report. Department of Civil Engineering, University of Mississippi. 143 p.

George, K. P. (2003). Falling Weight Deflectometer for estimating subgrade resilient moduli. Final report. Department of Civil Engineering, University of Mississippi. 113 p.

Grajewski, S. M. (2016). Influence of pavement moisture content on the load-bearing capacity of forest road. Infrastructure and Ecology of Rural Areas, 4(2), 1451–1462.

Grasty, R.L. 1997. Radon emanation and soil moisture effects on airborne gamma-ray measurements. Geophysics, 62:1379–1385. doi:10.1190/1.1444242.

Heidari, M.J.; Najafi, A.; Borges, J.G. Introducing New Index in Forest Roads Pavement Management System. Forests 2022, 13, 1674, doi:10.3390/f13101674.

Heiskanen, J., Hallikainen, V., Salmivaara, A., Uusitalo, J., Ilvesniemi, H. 2020. Predictive models to determine fine soil fractions and organic matter from readily available soil and terrain data of soils under boreal forest. Geo derma Reg. 20: e00251. doi:10.1016/j.geodrs.2019.e00251.

Herrmann, L., Schuler, U., Rangubpit, W., Erbe, P., Surinkum, A., Zarei, M., Stahr, K. 2010. The potential of gamma-ray spectrometry for soil map ping. In Proceedings of 19th World Congress of Soil Science, 1–6August2010, Brisbane, Australia. pp. 117–120.

Hoffmann, S., Schönauer, M., Heppelmann, J. *et al.* Trafficability Prediction Using Depth-to-Water Maps: the Status of Application in Northern and Central European Forestry. *Curr Forestry Rep* **8**, 55–71 (2022). doi:10.1007/s40725-021-00153-8

Hrůza, P., Mikita, T., Tyagur, N., Krejza, Z., Cibulka, M., Procházková, A., Patočka, Z. (2018). Detecting forest road wearing course damage using different methods of remote sensing. Remote Sensing, 10(4), 492. doi:10.3390/rs10040492

Huvstig, A. 2012. Model for the prediction of rutting in roads, a NordFoU result. Procedia – Social and Behavioral Sciences, 48, 2816–2826. doi:10.1016/j.sbspro.2012.06.1250

Hyvönen, E., Pänttäjä, M., Sutinen, M.-L., Sutinen, R. 2003. Assessing site suitability for Scots pine using airborne and terrestrial gamma-ray measurements in Finnish Lapland. Can. J. For. Res. 33(5): 796–806. doi:10.1139/x03-005.

Hyyppä, J., X. Yu, H. Hyyppä, and M. Maltamo. 2006. “Methods of Airborne Laser Scanning forForest Information Extraction.” In *International EARSeL Workshop 3D Remote Sensing inForestry Proceedings*, Vienna, Austria, February 14–15, 63–78.

Hyyppä, H., Yu, X., Hyyppä, J., Kaartinen, H., Kaasalainen, S., Honkavaara, E., Rönnholm, P. 2005. Factors affecting the quality of DTM generation in forested areas. Workshop *“Laser scanning 2005”* September 12th-14th, 2005. Working Group III/3. International Archives of Photogrammetry, Remote Sensing and Spatial Information Sciences, 36(3/W19), pp.85-90.

Hyyppä, H., Rönnholm, P., Hyyppä, J., Yu, X., Kaartinen, H. 2006. Laser Scanner Derived Digital Terrain Models for Highway Planning in Forested Areas. Nordic Journal of Surveying and Real Estate Research 3:1 (2006) 69–82

Immonen K., Kauppinen A., Kuru K., Tamminiemi M., Kallonen J., Strandström, M. 2000. Maanmuokkauksen koulutusaineisto. Metsäteho Oy, Helsinki, Finland. [In Finnish]

James, L. A., Watson, D. G., Hansen, W. F. (2007). Using LiDAR data to map gullies and headwater streams under forest canopy: South Carolina, USA. Catena, 71(1), 132–144. doi:10.1016/j.catena.2006.10.010

Kaakkurivaara T., Kolisoja P., Uusitalo J., Vuorimies N. (2016). Fly ash in forest road rehabilitation. Croatian Journal of Forest Engineering 37(1): 119–130.

Kaakkurivaara T., Korpunen H. (2017). Increased fly ash utilization – value addition through forest road reconstruction. Canadian Journal of Civil Engineering 44(3): 223–231. doi:10.1139/cjce-2016-0193

Kaakkurivaara, T., Uusitalo, J. (2011). Kelirikkoaikaisen puunkuljetuksen haasteet – ratkaisuja metsäteiden kuljetuskelpoisuuden ongelmiin sekä metsäteiden kantavuuden mittaukseen ja kunnostamiseen. Working Papers of the Finnish Forest Research Institute. doi:10.13140/RG.2.2.31965.00480

Kaakkurivaara, T., Vuorimies, N., Kolisoja, P., Uusitalo, J. (2015). Applicability of portable tools in assessing the bearing capacity of forest roads. Silva Fennica, 49(2), 1239. doi:10.14214/sf.1239

Kankare V., Luoma V., Saarinen N., Peuhkurinen J., Holopainen M., Vastaranta M. (2019). Assessing feasibility of the forest trafficability map for avoiding rutting – a case study. Silva Fennica vol. 53 no. 3 article id 10197. doi:10.14214/sf.10197

Karjalainen, T., Karjalainen, V., Waga, K., Tokola, T. (2024) Predicting the roadway width of forest roads by means of airborne laser scanning. International Journal of Applied Earth Observation and Geoinformation, Volume 133, 2024, 104109, ISSN 1569-8432, doi:10.1016/j.jag.2024.104109.

Klvac, R., Vrána, P., Jiroušek, R. (2010). Possibilities of using the portable falling weight deflectometer to measure the bearing capacity and compaction of forest soils. Journal of Forest Science. 56. 130-136. doi:10.17221/71/2009-JFS.

Kock P, Rääf C, Samuelsson C. 2014. On background radiation gradients – the use of airborne surveys when searching for orphan sources using mobile gamma-ray spectrometry. J Environ Radioact. 128:84–90. doi:10.1016/j.jenvrad.2013.10.022

Kock P, Samuelsson C. 2011. Comparison of airborne and terrestrial gamma spectrometry measurements –evaluation of three areas in southern Sweden. J Environ Radioact. 102(6):605–613. doi:10.1016/j. jenvrad.2011.03.010

Kogan, R.M., Nazarov, I.M., Fridman, S.D. 1971. Gamma spectrometry of natural environments and formations: theory of the method applications to geology and geophysics. Israel Program for Scientific Translations (IPST). p. 337.

Korpilahti, A. 2008. Metsätehon raportti 202: Metsäteiden kuntoinventoinnin ja kuntotiedon hyödyntämisen toimintamalli: 202. Metsäteho Oy. https://metsateho.fi/wp-content/uploads/2015/02/Raportti_202_AK.pdf

Kuhn, M., Wing, J., Weston, S., Williams, A., Keefer, C., Engelhardt, A., et al. 2020. caret: classification and regression training. R package version 6.0-86. Available from https://CRAN.R-project.org/package=caret.

Labelle, E., Jaeger, D. (2012). Quantifying the Use of Brush Mats in Reducing Forwarder Peak Loads and Surface Contact Pressures. Croatian Journal of Forest Engineering. 33. 249.

Lehtonen, I., Venäläinen, A., Kämäräinen, M., Asikainen, A., Laitila, J., Anttila, P., Peltola, H.: Projected decrease in wintertime bearing capacity on different forest and soil types in Finland under a warming climate, Hydrol. Earth Syst. Sci., 23, 1611–1631, doi:10.5194/hess-23-1611-2019, 2019.

Lidberg, W., Nilsson, M., Ågren, A. (2020). Using machine learning to generate high-resolution wet area maps for plan ning forest management:Astudyinaborealforestlandscape. Ambio,49(2), 475–486 doi:10.1007/s13280019-01196-9

Lideskog, H., Ersson, B.T., Bergsten, U., Karlberg, M. 2014. Determining boreal clearcut object properties and characteristics for identification purposes. Silva Fenn. 48(3): 1136. doi:10.14214/sf.1136.

Löf, M., Dey, D.C., Navarro, R.M., Jacobs, D.F. 2012. Mechanical site preparation for forest restoration. New For. 43(5–6): 825–848. doi:10.1007/s11056-012-9332-x.

Lundien, J.R. 1967. Terrain analysis by electromagnetic means: laboratory investigations in the 0- to 2.82-MeV gamma-ray spectral region. Technical report 3-693. U.S. Army Engineers Waterways Experiment Station, Vicks burg, Mississippi, USA. Available from https://hdl.handle.net/11681/32386.

Luoranen, J., Saksa, T., Finêr, L., Tamminen, P. 2007. Metsämaan Muokkausopas. Jyväskylä: Gummerus Kirjapaino Oy. [In Finnish.] Available from http://urn.fi/URN:ISBN:978-951-40-2059-9.

Malinen, J., Nousiainen, V., Palojärvi, K., Palander, T. (2014). Prospects and challenges of timber trucking in a changing operational environment in Finland. Croatian Journal of Forest Engineering, 35, 91–100.

Marchuk, S., Ostendorf, B. 2009. Relationship between soil properties and airborne GAMMA-radiometric data. In Proceedings of the Surveying and Spatial Sciences Institute Biennial International Conference, Adelaide 2009. Edited by B. Ostendorf, P. Baldock, D. Bruce, M. Burdett, and P. Corcoran. Surveying and Spatial Sciences Institute. pp. 1041–1051.

Mattila, U., Tokola, T. 2019. Terrain mobility estimation using TWI and airborne gamma-ray data. J. Environ. Manage. 232: 531–536. doi:10.1016/j.jenvman.2018.11.081. PMID:30503899.

Mehtätalo, L., Lappi, J. (2020). Biometry for forestry and environmental data: With examples in R. Chapman and Hall/CRC. doi:10.1201/9780429173462

Melander, L., Ritala, R., Strandström, M. 2019. Classifying soil stoniness based on the excavator boom vibration data in mounding operations. Silva Fenn. 53: 10068. doi:10.14214/sf.10068.

Metsäkeskus. 2023. Korjuukelpoisuuskartat. Harvest season maps. [accessed 2023 September 1st]. https://avoin.metsakeskus.fi/aineistot/ Korjuukelpoisuus/.

Minty, B.R.S. 1997. Fundamentals of airborne gamma-ray spectrometry. AGSO J. Aust. Geol. Geophys. 17 (2): 39–50.

Mohammadi S., Nikoudel M., Rahimi H., Khamehchiyan M. (2008). Application of the Dynamic Cone Penetrometer (DCP) for determination of the engineering parameters of sandy soils. Engineering Geology 101: 195–203. doi:10.1016/j.enggeo.2008.05.006

Moskalewicz D, Dzieduszyńska D, Elwirski Ł, Mroczek P, Petera- Zganiacz J, Tylmann K, Woźniak P. 2022. Recognition of sedimentary environments using handheld gamma-ray spectrometry in Pleistocene Fennoscandian ice sheet glaciogenic basin, northern and central Poland. Mar Petroleum Geol. 140:105679. doi:10.1016/j.marpetgeo.2022.105679

Murphy G., Firth J. G., Skinner M. F. (2004). Long-term impacts of forest harvesting related soil disturbance on log product yields and economic potential in a New Zealand forest. Silva Fennica vol. 38 no. 3 article id 416. doi:10.14214/sf.416

Murphy P.N.C., Ogilvie, J., Arp, P., 2009. Topographic modelling of soil moisture conditions: a comparison and verification of two models. European Journal of Soil Science. 60 (1) :94–109. doi:10.1111/j.1365-2389.2008.01094.x

Murphy, P.N.C., Ogilvie, J., Castonguay, M., Zhang, C., Meng, F.R., Arp, P.A. 2008. Improving forest operations planning through high-resolution flow-channel and wet-areas mapping. Forestry Chronicle 84: 568–574. doi:10.5558/tfc84568-4.

Murphy, P.N.C., Ogilvie, J., Connor, K., Arp, P.A. 2007. Mapping wetlands: A comparison of two different approaches for New Brunswick, Canada. Wetlands 27, 846–854 (2007). doi:10.1672/0277-5212(2007)27[846:MWACOT]2.0.CO;2

National Land Survey of Finland. (2021a). Laserscanning data 2008-2019. https://www.maanmittauslaitos.fi/en/maps-and-spatial-data/datasets-and-interfaces/product-descriptions/laser-scanning-data

National Land Survey of Finland. (2021b). 5p Laser scanning data 2020. https://www.maanmittauslaitos.fi/en/maps-and-spatial-data/expert-users/product-descriptions/laser-scanning-data-5-p

Natural Resources Institution of Finland 2024, https://www.luke.fi/fi/uutiset/hakatun-puun-kokonaismaara-pieneni-vuonna-2023-energiapuuta-korjattiin-ennatyksellisen-paljon Accessed: 1/2025

Palander, T., Kärhä, K. 2016. Development of computational model to predict rut formation using GIS for planning of wood harvesting on drained peat lands. Int. J. Adv. Eng. Manage. Sci. 2: 2040–2057

Peng, J., Tanguy, M., Robinson, E., Pinnington, E., Evans, J., Ellis, R., Cooper, E., Hannaford, J., Blyth, E., Dadson, S., 2021 Estimation and evaluation of high-resolution soil moisture from merged model and Earth observation data in the Great Britain. *Remote Sensing of Environment*, 264, 112610. 18, pp. doi:10.1016/j.rse.2021.112610

Pohjankukka, J., Nevalainen, P., Pahikkala, T., Hyvönen, E., Sutinen, R., Hänninen, P., Heikkonen, J. 2014. Arctic soil hydraulic conductivity and soil type recognition based on aerial gamma-ray spectroscopy and to pographical data. In Proceedings of the 22nd International Conference on Pat tern Recognition (ICPR 2014). Edited by M. Borga, A. Heyden, D. Laurendeau, M. Felsberg, and K. Boyer. IEEE. pp. 1822–1827. doi:10.1109/ICPR.2014.319.

Pohjankukka, J., Riihimäki, H., Nevalainen, P., Pahikkala, T., Ala-Ilomäki, J., Hyvönen, E., et al. 2016. Predictability of boreal forest soil bearing capacity by machine learning. J. Terramechanics, 68: 1–8. doi:10.1016/j.jterra.2016.09.001

Priori, S., Bianconi, N., Costantini, E. 2014. Can γ-radiometrics predict soil textural data and stoniness in different parent materials? A comparison of two machine-learning methods. Geoderma, 226–227: 354–364. doi:10.1016/j.geoderma.2014.03.012.

R Core Team. 2020. R: a language and environment for statistical computing. R Foundation for Statistical Computing, Vienna, Austria. Available from https://www.R-project.org/.

Rantala, J., Saarinen, V.-M., Hallongren, H. 2010. Quality, productivity and costs of spot mounding after slash and stump removal. Scand. J. For. Res. 25(6): 507–514. doi:10.1080/02827581.2010.522591.

Rawlins, B.G., Lark, R.M., Webster, R. 2007. Understanding airborne radiometric survey signals across part of eastern England. Earth Surf. Process Landforms, 32:1503–1515. doi:10.1002/esp.1468.

Rizzo, A., Antonacci, G., Borra, E., Cardellini, F., Ciciani, L., Sperandio, L., Vilardi, I. (2022). Environmental Gamma Dose Rate Monitoring and Radon Correlations: Evidence and Potential Applications. Environments. 9. 66. 10.3390/environments9060066.

Saarelainen, S., Makkonen, L., 2007. Seppo Saarelainen and Lasse Makkonen: Ilmastonmuutokseen sopeutuminen tienpidossa; Esiselvitys. (Finnish Transport Infrastructure Agency). Tiehallinnon selvityksiä 4/2007 [In Finnish]. Available Online:

https://ava.vaylapilvi.fi/ava/Julkaisut/Ava-palvelin/pdf/3201029-v-ilmastonmuutokseen_sopeutuminen_tienpidossa.pdf

Saarenketo, T., Aho, S. (2005). Managing spring thaw weakening on low volume roads: Problem description, load restriction policies, monitoring and rehabilitation 2005. Roadscanners Oy. https://www.roadex.org/wp-content/uploads/2014/01/ 2_3-Spring_Thaw_Weakening_l.pdf

Saarilahti, M. 2002. Soil interaction model. EU 5th Framework Project (Quality of Life and Management of Living Resources) Contract No. QLK5- 1999-00991 (1999-2002).

Saarilahti, M., Anttila, T. 1999. Rut depth model for timber transport of moraine soils. In Proceedings of the 9th International Conference of International Society for Terrain-Vehicle Systems (pp. 29–37). Available from http://hdl.handle.net/1975/8068.

Saarinen, V.-M. 2006. The effects of slash and stump removal on productivity and quality of forest regeneration operations – preliminary results. Biomass Bioenergy, 30(4): 349–356. doi:10.1016/j.biombioe.2005.07.014.

Sabouri, M., Khabiri, S., Asgharzadeh, S. M, Abdollahi, S. F. (2022). Investigating the performance of geogrid reinforced unbound layer using light weight deflectometer (LWD). International Journal of Pavement Research and Technology, 15, 173–183. doi:10.1007/s42947-021-00015-3

Saksa, T., Miina, J., Haatainen, H., Kärkkäinen, K. 2018. Quality of spot mounding performed by continuously advancing mounders. Silva Fenn. 52(2): 9933. doi:10.14214/sf.9933.

Salmivaara, A. (2020). Cartographic Depth-to-Water (DTW) index map, 2m. CSC– IT Center for Science Ltd. https://etsin.fairdata.fi/dataset/6169811e-1f16-452b-ad6d-efec78fc51f2

Salour, F., Erlingsson, S. (2012). Pavement Unbound Materials Stiffness-Moisture Relationship during Spring Thaw. Proceedings of the International Conference on Cold Regions Engineering. 402-412. doi:10.1061/9780784412473.040.

Sanderson, D.C.W., Cresswell, A.J., Lang, J.J., Scott, E.M., Lauritzen, B., Karlsson, S., Strobl, C., Karlberg, O., Winkelmann, I., Thomas, M. 2004. An international comparison of airborne and ground based gamma ray spectrometry. Results of the ECCOMAGS 2002 exercise held 24th May to 4th June 2002, Dumfries and Galloway, Scotland. Glasgow: University of Glasgow.

Schwarzer, T.F., Adams, J.A.S. 1973. Rock and soil discrimination by low altitude airborne gamma-ray spectrometry in Payne County, Oklahoma. Econ. Geol. 68: 1297–1312. doi:10.2113/gsecongeo.68.8.1297.

Siekmeier J., Pinta C., Merth S., Jensen J., Davich P., Camargo F., Beyer M. (2009). Using the Dynamic Cone Penetrometer and Light Weight Deflectometer for construction quality assurance. Minnesota Department of Transportation, MN/RC 2009-12. 50 p.

Simola, H., Pitkänen, A. Turunen, J. (2012), Carbon loss in drained forestry peatlands in Finland, estimated by re-sampling peatlands surveyed in the 1980s. European Journal of Soil Science, 63: 798-807. doi:10.1111/j.1365-2389.2012.01499.x

Sirén, M., Salmivaara, A., Ala-Ilomäki, J., Launiainen, S., Lindeman, H., Uusitalo, J., Sutinen, R., Hänninen, P. 2019. Predicting forwarder rut formation on fine-grained mineral soils. Scand J For Res. 34 (2):145–154. doi:10.1080/02827581.2018.1562567

Skorseth, K., Selim, A. (2000). GRAVEL ROADS: MAINTENANCE AND DESIGN MANUAL.

Stendahl, J., Lundin, L., Nilsson, T. 2009. The stone and boulder content of Swedish forest soils. Catena, 77 (3): 285–291. doi:10.1016/j.catena.2009.02.011.

Sterner, K., Edman, T., Fjeld, D. (2023). Transport management – a Swedish case study of organizational processes and performance. International Journal of Forest Engineering, 35(1), 67–74. doi:10.1080/14942119.2023.2202614

Suvinen, A. (2006). A GIS-based simulation model for terrain tractability. Journal of Terramechanics, 43(4), 427–449. doi:10.1016/j.jterra.2005.05.002

Suvinen, A., Tokola, T., Saarilahti, M. 2009. Terrain trafficability prediction with GIS analysis. For. Sci. 55: 433–442.

Takeuchi, N., Katase, A. (1982). Rainout-Washout Model for Variation of Environmental Gamma-Ray Intensity by Precipitation. *Journal of Nuclear Science and Technology*, *19*(5), 393–409. doi:10.1080/18811248.1982.9734160

Taylor, M., Smettem, K., Pracilio, G., Verboom, W. 2002. Relationships between soil properties and high-resolution radiometrics, central eastern Wheatbelt Western Australia. Explor. Geophys. 33: 95–102. doi:10.1071/EG02095.

Terratest. (2022). Model 6000 BLE. https://light-weight-deflectometer.com/#technical-details

Uotila, E., Viitala, E.-J. (2000). Tietiheys metsätalouden maalla [Forest road density in Finland]. Metsätieteen aikakauskirja, 2000(1), 19–33. doi:10.14214/ma.6910

Uusitalo, J., Ala-Ilomäki, J., Lindeman, H., Toivio, J., Siren, M. 2020. Predicting rut depth induced by an 8-wheeled forwarder in fine-grained boreal forest soils. Ann. For. Sci. 77: 42. doi:10.1007/s13595-020-009

Uusitalo, J., Salomäki, M., Ala-Ilomäki, J. 2015. The effect of wider logging trails on rut formations in the harvesting of peatland forests. Croat. J. For. Eng. 36: 125–130.

Varol, T., Ozel, H., Ertuğrul, M., Emir, T., Tunay, M., Çetin, M., Sevik, H. (2021). Prediction of soil-bearing capacity on forest roads by statistical approaches. Environmental Monitoring and Assessment. 193. doi:10.1007/s10661-021-09335-0.

Venäläinen, P., Alanne, H., Ovaskainen, H., Poikela, A., Strandström, M., 2018. Kausivaihtelun kustannukset ja vähentämiskeinot puun toimitusketjussa. Metsätehon tuloskalvosarja 8/2017. [In Finnish.] Available from http://www.metsateho.fi/kausivaihtelun-kustannukset-ja-vahentamiskeinot/.

Viitala, E.-J., Saarinen, V.-M., Mikkola, A., Strandström, M. (2004). Metsäteiden lisärakentamistarpeen määrittäminen paikkatietoaineistojen avulla. Metsätieteen aikakauskirja, 2004(2), 6247. [In Finnish]. doi:10.14214/ma.6247

Viro, P. 1952. Kivisyyden määrittäminen. Communicationes Instituti Forestalis Fenniae, 40(3).

Viro, P.J. 1947. The mechanical composition and fertility of forest soil taking into consideration especially the stoniness of the soil. Communicationes Instituti Forestalis Fenniae, 25(2)

Viro, P.J. 1958. Suomen metsämaiden kivisyydestä. Summary: Stoniness of forest soil in Finland. Communicationes Instituti Forestalis Fenniae, 49(4): 45.

Vuorimies N., Kolisoja P., Kaakkurivaara T., Uusitalo J. (2015). Estimation of risk for rutting on forest roads during thawing period of seasonal frost. Transportation Research Record: Journal of the Transportation Research Board 2474: 143–148. doi:10.3141/2474-17

Vuorimies, N., Kurki, A., Kolisoja, P., Varin, P., Saarenketo, T., Pekkala V., Haataja M. 2019. Tierakenteen rasittuminen yli 76 tonnin HCT-yhdistelmien koekuormituksissa vuosina 2015–2018. (Finnish Transport Infrastructure Agency). Väyläviraston tutkimuksia 21/2019. ISSN 2490- 0982, ISBN 978-952-317-745-1. [In Finnish]. Available Online: https://julkaisut.vayla.fi/pdf12/vt_2019-21_tierakenteen_rasittuminen_web.pdf

Waga, K., Malinen, J., Tokola, T. (2015). Forest road quality control using ALS data. Canadian Journal of Forest Research, 45(11), 1636–1642. doi:10.1139/cjfr-2015-0067

Waga, K., Malinen, J., Tokola, T. (2016). Comparison of high and low density airborne lidar data for forest road quality assessment. ISPRS Annals of the Photogrammetry, Remote Sensing and Spatial Information Sciences, III-8, 167–172. doi:10.5194/isprs-annals-III-8-167-2016

Waga, K., Malinen, J., Tokola, T. (2020). A topographic wetness index for forest road quality assessment: An application in the Lakeland Region of Finland. Forests, 11(11), 1165. doi:10.3390/f11111165

Waga, K., Malinen, J., Tokola, T. (2021). Locally invariant analysis of forest road quality using two different pulse density airborne laser scanning datasets. Silva Fennica, 55(1), 10371. doi:10.14214/sf.10371

Wilford, J., Minty, B. 2006. The use of airborne gamma-ray imagery for mapping soils and understanding landscape processes. Dev. Soil Sci. 31: 207–218. doi:10.1016/S0166-2481(06)31016-1.

Wingate-Hill, R. Jakobsen, B.F. 1982. Increased mechanisation and soil damage in forests - A review. N. Z. J. For. Sci.. 12. 380-393.

Wong, M.T.F., Harper, R.J. 1999. Use of on-ground gamma-ray spectrometry to measure plant-available potassium and other topsoil attributes. Soil Res. 37(2): 267–278. doi:10.1071/S9803d8.